Early-Life Exposure to DBP and DEHP Induces Ultrastructural Testicular Damage and Semen Quality Deterioration Through Modulation of Inhibin-α, Calretinin, and PPAR-γ Expression

Reda A Ali, Heba E Aboulqasem, Ekbal T Wassif, Dalia Elzahraa F Mostafa

DECTRIS QUADRO

The flexible standard for **electron microscopy**
Maximizing performance on a single platform



Downloaded from academic.oup.com/mam/article/32/6/ozag107/8979578 by Ragesh Nair Nair on 17 November 2026

Microscopy and Microanalysis, 2026, **32**, ozag107
https://doi.org/10.1093/mam/ozag107
Advance access publication 22 October 2026
Original Article

Microscopy AND Microanalysis

Early-Life Exposure to DBP and DEHP Induces Ultrastructural Testicular Damage and Semen Quality Deterioration Through Modulation of Inhibin-α, Calretinin, and PPAR-γ Expression

Reda A. Ali, Heba E. Aboulqasem*, Ekbal T. Wassif, and Dalia Elzahraa F. Mostafa

Zoology & Entomology Department, Faculty of Science, Assiut University, Assiut 71516, Egypt

***Corresponding author:** Heba E. Aboulqasem, E-mail: Heba.El-sayed@science.aun.edu.eg

Abstract

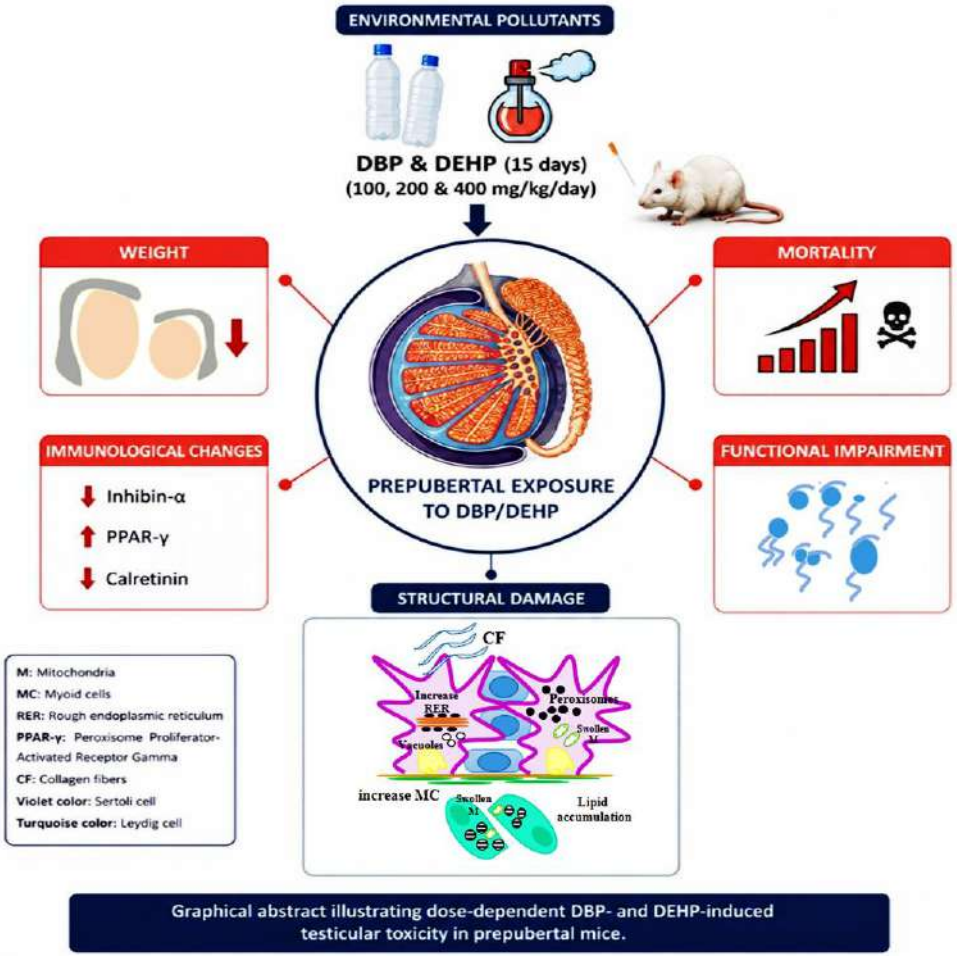
Phthalates, including dibutyl phthalate (DBP) and di-2-ethylhexyl phthalate (DEHP), are plasticizers causing male reproductive toxicity. This study investigated early pubertal exposure in ninety-six immature male Swiss albino mice administered DBP or DEHP (100, 200, and 400 mg/kg) for 15 days, evaluated at 36, 45, 50, and 70 days to assess both exposure effects and recovery. Light microscopy of Hematoxylin and Eosin-stained sperm smears and transmission electron microscopy (TEM), alongside immunohistochemical investigations for inhibin-α, calretinin, and peroxisome proliferator-activated receptor gamma (PPAR-γ), were utilized. Exposure induced severe, dose-dependent toxicity, causing complete sperm absence at 36 days, followed by reduced viability (~20%) and teratozoospermia (>80%). TEM revealed extensive ultrastructural damage; mitochondrial degeneration reached 37% (DBP-400) and 47.9% (DEHP-400), while Sertoli cell vacuolization averaged ~8 and ~5 vacuoles/cell in high-dose groups. Concurrently, disrupted lipid homeostasis was evidenced by peroxisome proliferation and increased Leydig lipid area fraction, exceeding 50% in the DBP-400 group by 50 days. Recovery at 70 days was dose-dependent, occurring primarily in low-dose groups following treatment withdrawal. Immunohistochemical investigations demonstrated decreased inhibin-α and calretinin expression, alongside increased PPAR-γ immunoreactivity. Early-puberty phthalate exposure was associated with mitochondrial injury, altered PPAR-γ expression, disrupted lipid homeostasis, and incomplete recovery of testicular alterations at higher doses.

Key words: mitochondria, peroxisomes, phthalate, teratozoospermia, testis, vacuolization

Downloaded from academic.oup.com/mam/article/32/6/ozag107/8979578 by Ragesh Nair Nair on 17 November 2026

Received: March 26, 2026. **Revised:** September 1, 2026. **Accepted:** September 11, 2026
© The Author(s) 2026. Published by Oxford University Press on behalf of the Microscopy Society of America. All rights reserved. For commercial re-use, please contact reprints@oup.com for reprints and translation rights for reprints. All other permissions can be obtained through our RightsLink service via the Permissions link on the article page on our site—for further information please contact journals.permissions@oup.com.

Graphical abstract



Graphical abstract illustrating dose-dependent DBP- and DEHP-induced testicular toxicity in prepubertal mice.

Introduction

Over the past five decades, a 32.5% decline in sperm concentration in men has been reported. This decline mirrors a significant reduction in total fertility rates in many countries, particularly in highly developed regions such as Eastern Asia and Europe (Aitken, 2024). Among the various factors contributing to this trend, increasing exposure to environmental pollutants has raised substantial concern. In particular, endocrine-disrupting chemicals, such as phthalates, have been shown to adversely affect male reproductive health (Sharma et al., 2020).

Phthalate esters (PAEs), commonly known as phthalates, are a group of synthetic, colorless, viscous, and lipophilic liquid compounds that are esters formed from phthalic acid and various alcohols. They are mainly used as plasticizers, additives incorporated into polymers like polyvinyl chloride to enhance flexibility, clarity, strength, and lifespan (Li et al., 2019). They are also incorporated into cosmetics as fragrance carriers and are present in numerous consumer products, including children's toys, and medical devices. Due to their extensive use, human exposure to phthalates is nearly ubiquitous, raising significant public health concerns, especially for vulnerable populations. For instance, substantial amounts of phthalates (up to 5%) are used in cosmetics and personal care products, and daily application of these products has been associated with a rapid increase in urinary concentrations of phthalate monoesters (Huang et al., 2018). Global production of PAEs has increased dramatically over the past decades (Prasad, 2021). More recent estimates indicated that the annual production of PAEs had reached ~5–8 million tons by 2016, reflecting the continued expansion of their industrial use (Wowkonowicz, 2023). Among these compounds, di-2-ethylhexyl phthalate (DEHP) and dibutyl phthalate (DBP) account for more than 60% of the global market share (Benjamin et al., 2017). It is estimated that at least 1 million tons of DEHP may have entered the Polish market since its production began in 1963 (Wowkonowicz, 2023). Owing to their high production volumes, extensive applications, and potential for widespread human exposure, DEHP and DBP were selected as the target compounds to evaluate their potential impact in the present study.

PAEs are bound to polymer chains only through weak van der Waals forces and hydrogen bonds. Therefore, they can easily leak into the environment, contributing to widespread human exposure and ecological contamination (Dong et al., 2025). Phthalates enter the human body primarily through

Downloaded from academic.oup.com/mam/article/32/6/ozag107/8979578 by Ragesh Nair Nair on 17 November 2026

ingestion, but inhalation and dermal absorption also represent important routes of exposure. Previous studies have linked phthalate exposure to adverse effects on multiple organ systems, including the endocrine, reproductive, urinary, nervous, cardiovascular, and digestive systems (Li et al., 2024). The male reproductive system is considered a primary target of phthalate toxicity, with evidence implicating disrupted testosterone synthesis, oxidative stress, and testicular dysfunction (Yang et al., 2025). Furthermore, recent human studies have reported that occupational exposure to phthalates is associated with alterations in reproductive hormone levels, suggesting potential disturbances of the hypothalamic–pituitary–gonadal axis (Nita et al., 2026).

The reproductive toxicity of phthalates has been widely documented in mammalian and avian testes; however, most studies have focused on prenatal, neonatal, or adult exposure stages, while early pubertal exposure remains less explored (Zakariah et al., 2025). This developmental window is critical as it involves Sertoli cell maturation and the initiation of active spermatogenesis, rendering the testes highly sensitive to endocrine disruption (Rey, 2021; Wang et al., 2022; Zakariah et al., 2025). Therefore, the aim of the present study was to investigate the effects of early pubertal exposure to DBP and DEHP on testicular structure and function in immature male mice, and to evaluate the potential reversibility of these effects after cessation of exposure using functional, ultrastructural, and immunohistochemical approaches.

Material and Methods

Chemicals

DEHP and DBP, with 98% purity, were purchased from SRL (India). The chemicals were miscible in corn oil (used as a vehicle) before administration and were stored at room temperature.

Experimental Animals

A total of 96 immature male albino mice (Swiss strain), aged 21 days and weighing 8–12 g on average, were obtained from the Animal House of the Faculty of Science, Al-Azhar University, Assiut. Animals were maintained under controlled environmental conditions (23 ± 2°C; 12 h light/dark cycle) with food and water provided *ad libitum*. The mice were divided into eight groups: a control group, a corn oil (vehicle) group, and six treatment groups. The treated groups received a daily oral dose of 100 μL corn oil containing DBP or DEHP at three dose levels (100, 200, and 400 mg/kg) for 15 consecutive days (Fig. 1). In accordance with institutional and international guidelines for the care and use of laboratory animals, twelve mice from each group were euthanized by cervical dislocation at four developmental time points (36, 45, 50, and 70 days of age; $n = 3$ per time point). Body and testis weights were recorded at all designated time points, while mortality was monitored continuously from the beginning of the dosing period until 70 days of age. All recorded deaths occurred during the 15-day dosing period, and deceased animals were replaced to maintain equal sample sizes across the experimental groups. Semen analysis was performed at 36, 45, 50, and 70 days of age. Immunohistochemical assessment was conducted at 36 and 70 days of age, while ultrastructural evaluation was performed at 36 and 50 days of age. The selected time points represent key stages of murine testicular development, specifically early puberty and active spermatogenesis (Rey, 2021; Wang et al., 2022). The time point at 36 days of age was selected to assess the immediate effects of the 15-day exposure period, whereas the time points at 45, 50, and 70 days of

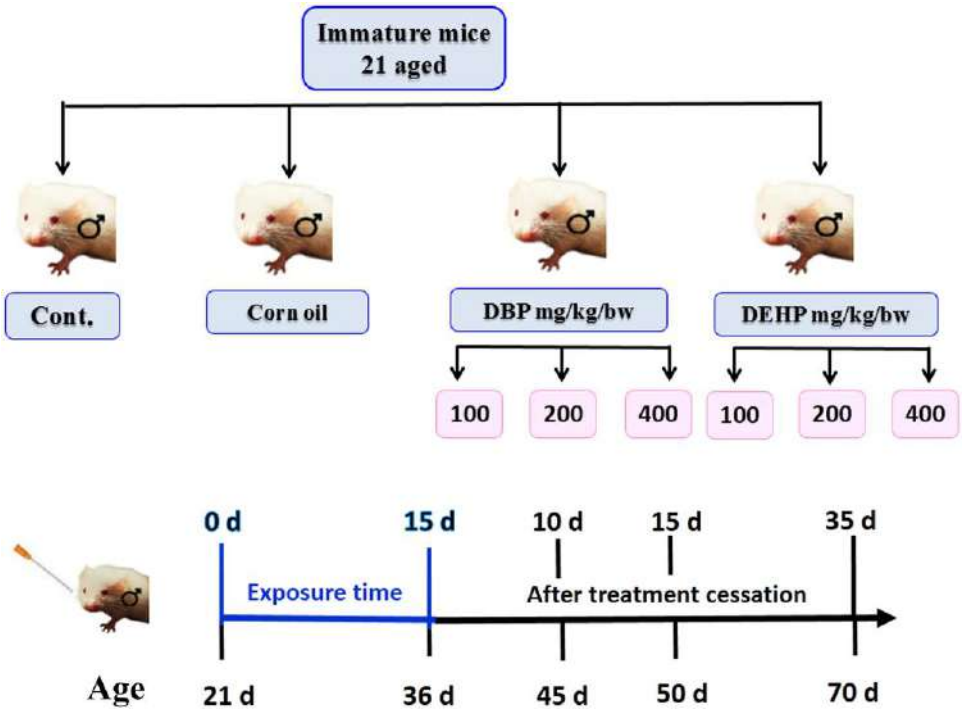


Fig. 1. Schematic representation of the experimental design illustrating the control and treated groups and the different dosing regimens of DEHP and DBP, as well as the ages selected for animal sacrifice and evaluation.

Downloaded from academic.oup.com/mam/article/32/6/ozag107/8979578 by Ragesh Nair Nair on 17 November 2026

age were used to evaluate potential recovery following treatment cessation.

Dose Selection

Doses of DBP and DEHP (100, 200, and 400 mg/kg) were selected based on previous rodent studies demonstrating reproductive and histopathological toxicity (Wang et al., 2021; Reddy et al., 2025). Although these doses exceed typical environmental human exposure levels (Eslami et al., 2025), phthalates are encountered through multiple sources, resulting in chronic cumulative exposure over time (Al-Saleh & Elkhatib, 2016). Therefore, these doses were used to characterize the toxicological effects of DBP and DEHP under controlled experimental conditions.

Sperm Parameters Assessment

For sperm count and motility assessment, mice from all groups were euthanized by cervical dislocation. The right and left testes and epididymides were isolated. As previously described, spermatozoa were obtained from the cauda epididymis of each group (Verma & Singh, 2014). The cauda epididymis was cut with a fine needle and maintained in a saline solution at 37°C. The tissue was then thoroughly minced with sterile scissors to release the sperm into the saline. After dilution in normal saline (1:20), a 10 μL spermatozoa suspension was used to evaluate sperm concentration and motility using a Neubauer hemocytometer, following standard experimental procedures for rodent sperm analysis (Strader et al., 1996).

For sperm morphology assessment, smears were prepared immediately after sperm collection and fixed with methanol. The slides were stained with hematoxylin and eosin, examined under a light microscope at ×1,000 magnification, and photographed using an OPTICA microscope (Italy) equipped with a digital camera. A total of 100 spermatozoa per sample were evaluated and scored as either normal or abnormal according to strict morphological criteria. Morphological abnormalities were categorized as head, tail, and midpiece defects. The percentage of normal and abnormal spermatozoa was then estimated.

To determine sperm viability, the Eosin-Nigrosin staining method was used. Unstained (white) sperm heads were considered viable (live), whereas pink or red-stained heads were classified as nonviable (dead). Approximately 100 spermatozoa were examined under light microscope at ×400 magnification in each counting chamber to minimize deviation (Seed et al., 1996).

Transmission Electron Microscopic Investigations

Small specimens of the testis at 36 and 50 days of age were fixed in 2.5% glutaraldehyde and 2.5% paraformaldehyde in 0.1 M sodium cacodylate buffer, pH 7.3, and left overnight at 4°C. Samples were postfixed in 1% osmic acid in 0.1 M sodium cacodylate for 2 h at room temperature, dehydrated in ethanol, and embedded in an Araldite-Epon mixture. Semi-thin sections (1 μm in thickness) were stained with toluidine blue and examined under light microscope. Ultrathin sections were stained with uranyl acetate and lead citrate before examination under a JEOL100 II transmission electron microscope (TEM) (Reynolds, 1963).

Ultrastructural quantification was performed on TEM micrographs using ImageJ software. Mitochondria exhibiting swelling and disrupted cristae were considered damaged. The percentage of damaged mitochondria was calculated relative to the total mitochondrial count in each micrograph.

$$\text{Damaged mitochondria (\%)} = \frac{\text{Number of damaged mitochondria}}{\text{Total mitochondria}} \times 100$$

Cytoplasmic vacuoles were also counted, and Sertoli cell vacuolization was expressed as number of vacuoles per cell.

$$\text{Sertolicellvacuolization (vacuoles/cell)} = \frac{\text{Total number of vacuoles}}{\text{Number of Sertoli cells}}$$

Lipid area fraction (%) was quantified by measuring the total lipid droplet area relative to the total cytoplasmic area.

$$\text{Lipidareafraction (\%)} = \frac{\text{Lipid droplet area}}{\text{Total cytoplasmic area}} \times 100$$

Immunohistochemical Investigation

The immunohistochemical investigation was carried out on formalin-fixed testes collected at 36 and 70 days of age. The specimens were processed and embedded in paraffin, and the tissue sections were cut at 4 μm. Sections were subjected to antigen retrieval using Tris–ethylenediaminetetraacetic acid buffer (pH 9.0) at 90°C for 20 min. The block of endogenous peroxidase was done by incubating the sections with 3% H_2O_2, followed by preincubation overnight at 4°C in 1% bovine serum albumin in PBS. The sections were stained for 30 min at 37°C, using the following antibodies that showed reactivity in mouse species: a rabbit monoclonal anti-Inhibin-α (1:200; Quartett, Berlin, Germany; Cat. No. QR088), a rabbit polyclonal anti-PPAR-γ (1:200; ABclonal Technology, Wuhan, China; Cat. No. A0270), and a rabbit monoclonal anti-Calretinin (1:200; Quartett, Berlin, Germany; Cat. No. QR059), according to the method described previously (Hsu et al., 1981). Sections were counterstained with hematoxylin. Images were captured using an Olympus microscope equipped with an Olympus EP50 digital camera. In parallel, tissue specimens, in which the primary antibodies were omitted and replaced with buffer, served as negative controls. Immunostaining was quantified using ImageJ software (Java SE Runtime Environment, version 6) in 10 randomly selected nonoverlapping fields of equal area containing seminiferous tubules per animal. The mean value obtained from the 10 fields for each animal was used for statistical analysis.

Statistical Analysis

Data were expressed as mean ± SE. Statistical analysis was performed using one-way ANOVA for comparisons within each age, and two-way ANOVA for comparisons involving both age and treatment effects. Tukey's multiple comparisons test was used as a *post hoc* test where appropriate. Statistical analyses were carried out using GraphPad Prism software for Windows, version 5.0 (GraphPad Software, Inc., San Diego, CA, USA), and Microsoft Excel (Microsoft Office 10). Optical density (OD) was analyzed using ImageJ software (Java SE Runtime Environment, version 6).

Results

The control and corn oil groups showed comparable values throughout the study, confirming the suitability of corn oil as a vehicle control. Body weights were comparable among all groups at 21 days of age. From 36 days of age onward, body weight significantly decreased in both DBP- and DEHP-treated groups compared with the control ($p < 0.001$), with the greatest reductions observed in the 400 mg/kg groups of both compounds (Fig. 2a). Age-related analysis showed a progressive increase in body weight in both control groups from 21 to 70 days of age, whereas high-dose phthalate exposure markedly impaired this growth pattern. DBP (400 mg/kg)

Downloaded from academic.oup.com/mam/article/32/6/ozag107/8979578 by Ragesh Nair Nair on 17 November 2026

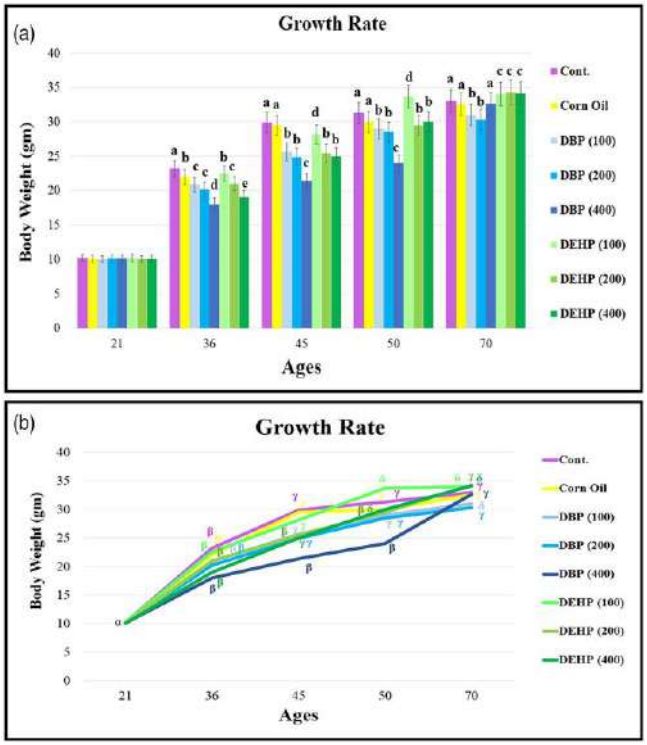


Fig. 2. Body weight gain in control and DBP- and DEHP-treated groups (100, 200, and 400 mg/kg) at different developmental ages. (**a**) Comparisons among experimental groups. Different Latin letters indicate significant differences between groups ($p < 0.05$). (**b**) Changes across developmental ages. Different Greek letters indicate significant differences between developmental ages ($p < 0.05$).

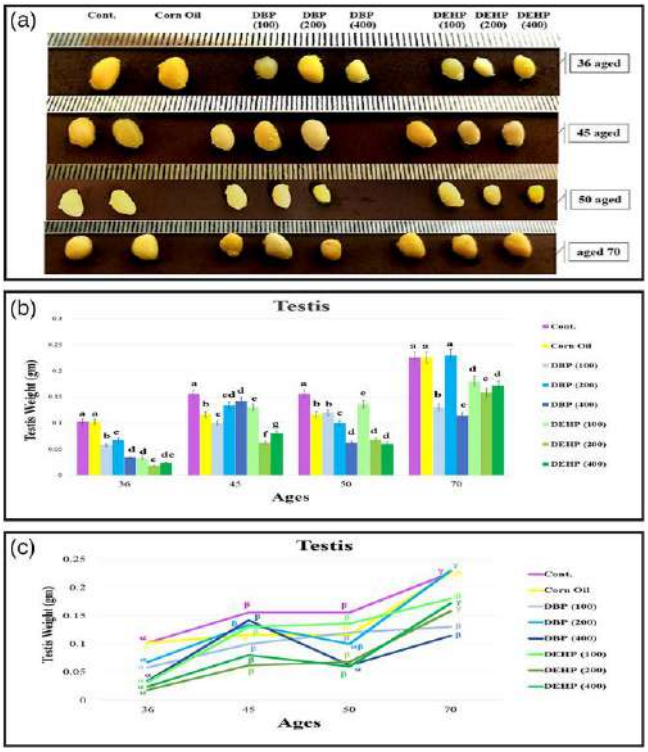


Fig. 3. (**a**) Comparative photographs of testes from control, corn oil, DBP, and DEHP-exposed groups (100, 200, and 400 mg/kg) at four ages. (**b**) Comparisons of testis weight among experimental groups. Different Latin letters indicate significant differences between groups ($p < 0.05$). (**c**) Comparisons of testis weight among developmental ages. Different Greek letters indicate significant differences between ages ($p < 0.05$).

showed limited weight gain between 36 and 50 days of age, while DEHP-treated groups exhibited partial recovery from 50 days of age, approaching control values by 70 days of age. In contrast, DBP-treated groups maintained reduced body weights throughout the experimental period (Fig. 2b). Two-way ANOVA confirmed significant effects of age, treatment, and their interaction, indicating that the effect of DBP and DEHP on body weight varied across developmental ages.

Testis weight significantly decreased at 36 and 45 days of age in all treated groups ($p < 0.001$), particularly in DEHP (400 mg/kg) group (Figs. 3a, 3b). Age-related analysis revealed a progressive increase in testis weight in control group, reaching the highest values at 70 days of age. Two-way ANOVA demonstrated significant effects of age, treatment, and their interaction, confirming that phthalate-induced alterations in testis growth were age- and dose-dependent. Phthalate-treated groups showed impaired testicular growth, especially DBP (400 mg/kg), which exhibited minimal changes between 36 and 50 days of age. By 70 days of age, lower-dose DBP and DEHP groups (100 and 200 mg/kg) showed partial recovery, with testis weights approaching control values (Fig. 3c).

Cumulative mortality throughout the experimental period was minimal in both the control (5%) and corn oil (6.66%) groups. In contrast, DBP-treated groups showed a progressive rise in mortality across doses: DBP (400 mg/kg) recorded the highest value (28%), followed by DBP (200 mg/kg) (27.58%), and DBP (100 mg/kg) (25.8%). All DEHP-treated groups displayed comparable moderate mortality levels (22.22% each) (Fig. 4).

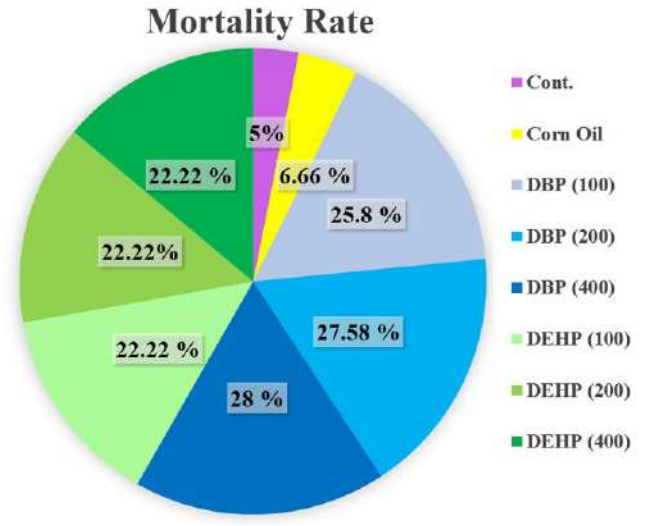


Fig. 4. Percentage of mortality rate across control, corn oil, DBP, and DEHP-exposed groups (100, 200, and 400 mg/kg).

Semen Analysis

Sperm Concentration

At 36 days of age, sperm concentration was only measurable in the control groups. In all treatment groups DBP and DEHP (100, 200, and 400 mg/kg), sperm concentration was undetectable, indicating a severe impairment in spermatogenesis due to

Downloaded from academic.oup.com/mam/article/32/6/ozag107/8979578 by Ragesh Nair Nair on 17 November 2026

both DBP and DEHP exposure, even at the lowest dose (Fig. 5a).

Sperm concentration in control group increased at 45 and 50 days of age relative to the values recorded at 36 days. Notably, low and medium doses (100 and 200 mg/kg) of DBP and DEHP showed significantly reduced concentrations compared with control at both 45 and 50 days of age ($p < 0.0001$; $F(7,72) = 579.4$; $\eta p^2 = 0.98$) and ($p < 0.0001$; $F(7,72) = 462.7$; $\eta p^2 = 0.98$), respectively, while high doses (400 mg/kg) of both DBP and DEHP resulted in complete absence of sperms (Figs. 5b, 5c).

At 70 days of age, sperm concentration improved across all groups compared with values observed at 50 days of age, indicating partial recovery. The control and (100 mg/kg) doses of both DBP and DEHP maintained high sperm concentrations, with insignificant differences among them ($p > 0.05$). However, both DBP and DEHP (200 and 400 mg/kg) exhibited a significant, dose-dependent decrease in sperm concentration ($p < 0.0001$; $F(7,72) = 610.7$; $\eta p^2 = 0.98$), with the 400 mg/kg dose exerting the most pronounced reduction (Fig. 5d).

Two-way ANOVA revealed significant effects of age, treatment, and their interaction ($p < 0.0001$), indicating that sperm concentration recovery differed according to both exposure dose and age after treatment withdrawal. The control group maintained the highest sperm concentrations throughout the study, with a progressive age-dependent increase from day 36 to 70 days of age. In contrast, DBP and DEHP exposure induced dose-dependent reductions in sperm concentration, with distinct recovery patterns among treated groups. In the low-dose groups (100 mg/kg) for both DBP and DEHP, sperm concentration progressively increased after the initial decline at 36 day of age, reaching significantly comparable levels to controls by 70 days of age. The mid-dose groups (200 mg/kg) for both DBP and DEHP showed significant delayed reduction through 36–50 days of age before a partial increase at 70 days of age, although values remained significantly lower than control levels. In the high-dose groups (400 mg/kg) for both DBP and DEHP, spermatogenesis was severely impaired with minimal recovery up to 50 days of age; despite a significant increase at 70 days of age, values remained significantly lower than controls, indicating persistent impairment (Fig. 5e).

Sperm Motility

At 45 and 50 days of age, sperm motility was significantly reduced in DBP and DEHP-treated groups compared with control ($p < 0.0001$; $F(5,54) = 239$; $\eta p^2 = 0.96$) and ($p < 0.0001$; $F(5,54) = 379.4$; $\eta p^2 = 0.97$) respectively. Control group exhibited the highest sperm motility values. In contrast, DBP and DEHP (100 mg/kg) caused significant reductions in motility, while the (200 mg/kg) dose of both compounds resulted in immotile sperms, with an insignificant difference between them. These results demonstrate a dose-dependent negative effect of both DBP and DEHP on sperm motility (Figs. 6a, 6b).

At 70 days of age, DBP exposure resulted in a dose-dependent decline: DBP (100 mg/kg) significantly reduced motility compared with control, with further decreases at (200 and 400 mg/kg). Similarly, DEHP (100 mg/kg) also showed a significant reduction but was still higher than the DBP-treated groups ($p < 0.0001$; $F(7,72) = 142.7$; $\eta p^2 = 0.93$).

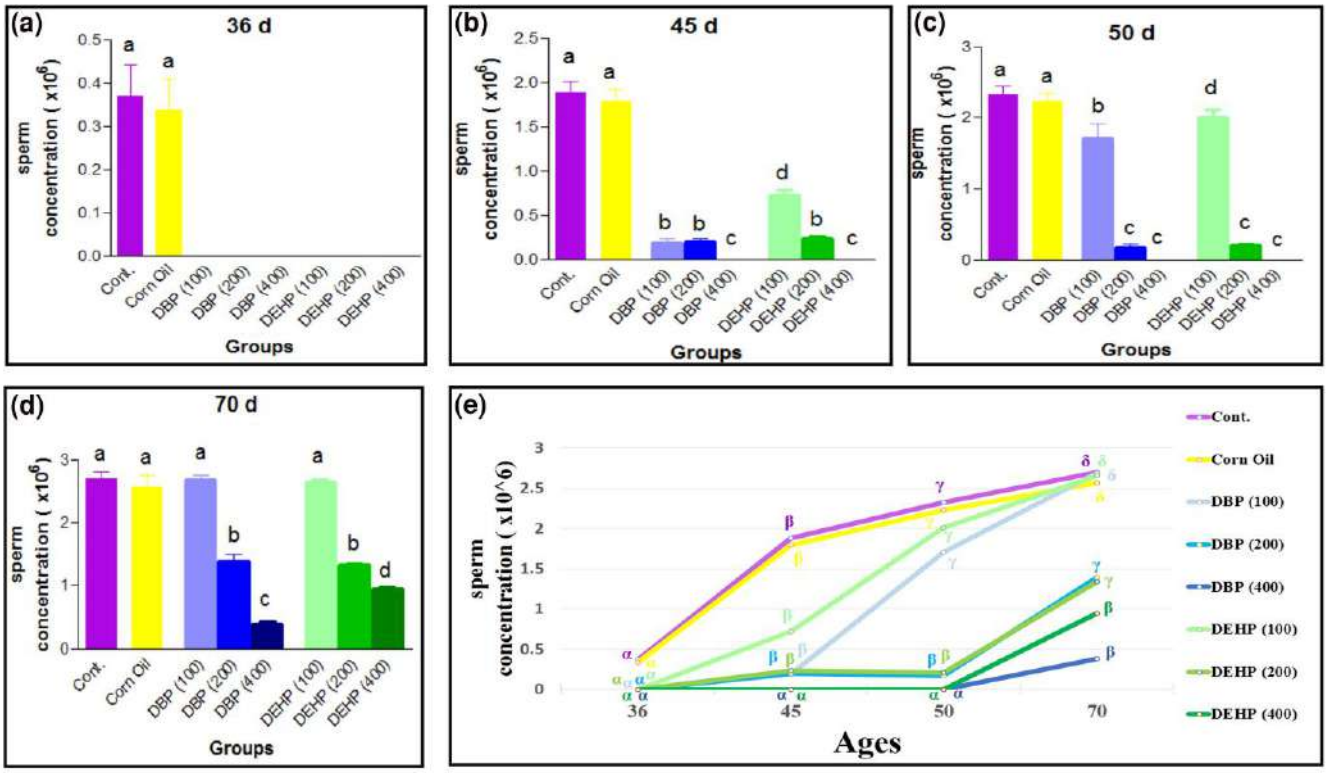


Fig. 5. Sperm concentration (×10^6) in control and DBP- and DEHP-exposed groups (100, 200, and 400 mg/kg). (**a**–**d**) Sperm concentration measured at different ages: (**a**) 36 days of age, (**b**) 45 days of age, (**c**) 50 days of age, and (**d**) 70 days of age. (**e**) Line graph illustrating changes in sperm concentration across different ages (36, 45, 50, and 70 days) throughout the experimental period in control and treated groups. Different Latin letters indicate significant differences between experimental groups, while Greek letters indicate significant differences between developmental ages ($p < 0.05$).

Downloaded from academic.oup.com/mam/article/32/6/ozag107/8979578 by Ragesh Nair Nair on 17 November 2026

DEHP (200 and 400 mg/kg) led to progressively lower motility, with the 400 mg/kg dose showing the greatest impairment. These findings indicate that both DBP and DEHP significantly impaired sperm motility in a dose-dependent manner, with DEHP at lower doses showing slightly less reduction than DBP (Fig. 6c).

Sperm Viability

At 45 days of age, sperm viability remained high in control group. DBP (100 and 200 mg/kg) showed significantly reduced viability, while DEHP-treated groups exhibited distinct responses: DEHP (100 mg/kg) showed a value significantly lower than control ($p < 0.0001$; $F(5,54) = 163.6$; $\eta p^2 = 0.94$) but higher than the DBP groups, whereas DEHP (200 mg/kg) insignificantly differed from the DBP groups (Fig. 7a).

At 50 days of age, sperm viability was significantly reduced in DBP and DEHP groups compared with control group ($p < 0.0001$; $F(5,54) = 63.02$; $\eta p^2 = 0.85$). DBP causing the most pronounced significant decrease in a dose-dependent manner. DEHP exposure also significantly lowered viability, but its effects were generally less severe than those of DBP (Fig. 7b).

At 70 days of age, sperm viability showed an improvement compared with earlier ages. The control group exhibited high sperm viability, with an insignificant difference between them ($p > 0.05$). DBP (100 mg/kg) resulted in a significant decrease in viability ($p < 0.05$), while (200 and 400 mg/kg) doses caused further reductions. Similarly, DEHP (100 mg/kg) led to a significant decrease in sperm viability, and the (200 and 400 mg/kg) doses resulted in more reductions. Although sperm viability remained significantly reduced in the DBP and DEHP groups compared with control ($p < 0.0001$; $F(7,72) = 165$; $\eta p^2 = 0.94$), the overall improvement in viability at 70 days suggests partial recovery from the effects observed at earlier ages and a dose-dependent effect of the two compounds (Fig. 7c).

Teratozoospermia

At 45 and 50 days of age, teratozoospermia was significantly higher in the DBP and DEHP treatment groups compared with the control group ($p < 0.0001$; $F(5,54) = 117.10$; $\eta p^2 = 0.92$) and ($p < 0.0001$; $F(5,54) = 118.6$; $\eta p^2 = 0.92$) respectively. The control group showed the lowest levels of teratozoospermia, with an insignificant difference among them. Both DBP

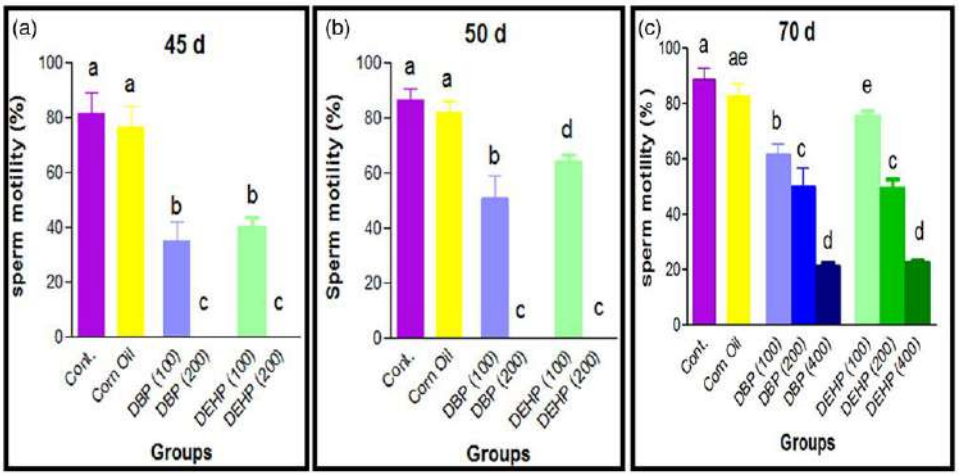


Fig. 6. Sperm motility in control, DBP, and DEHP-exposed groups (100, 200, and 400 mg/kg). Different Latin letters indicate significant differences between groups ($p < 0.05$). (**a**) At 45 days of age, (**b**) at 50 days of age, and (**c**) at 70 days of age.

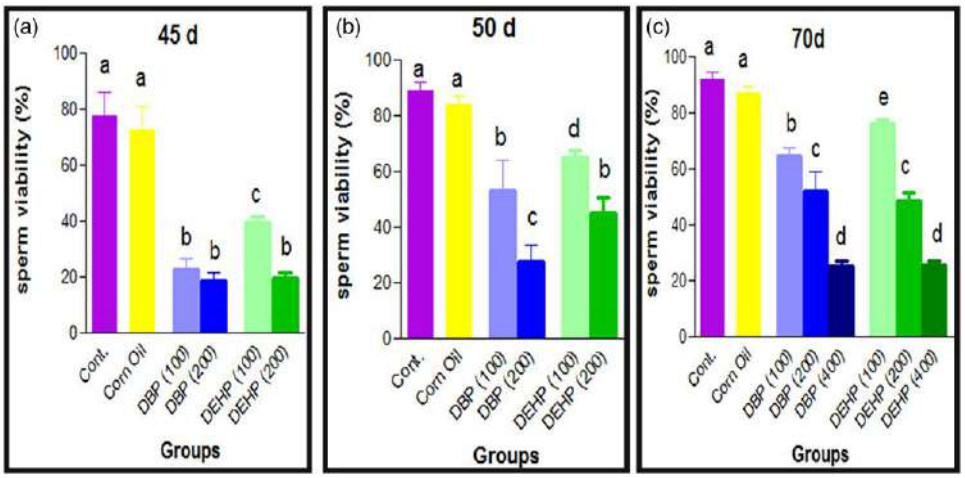


Fig. 7. Sperm viability in control, DBP, and DEHP-exposed groups (100, 200, and 400 mg/kg). Different Latin letters indicate significant differences between groups ($p < 0.05$). (**a**) At 45 days of age, (**b**) at 50 days of age, and (**c**) at 70 days of age.

Downloaded from academic.oup.com/mam/article/32/6/ozag107/8979578 by Ragesh Nair Nair on 17 November 2026

and DEHP (100 and 200 mg/kg) led to a significant increase in teratozoospermia, with an insignificant difference among doses within each chemical ($p > 0.05$) (Figs. 8a, 8b).

At 70 days of age, teratozoospermia was significantly higher in all DBP and DEHP treatments compared with control ($p < 0.0001$; $F(7,72) = 47.2$; $\eta p^2 = 0.82$). DBP and DEHP at all doses (100, 200, and 400 mg/kg) resulted in similar significant increases in teratozoospermia, with insignificant differences among doses within each chemical ($p > 0.05$). These results suggest that both DBP and DEHP exposure significantly elevated teratozoospermia in a dose-independent manner at 70 days (Fig. 8c).

Sperm Morphological Abnormalities

Mouse spermatozoa are composed of three main regions: the head, midpiece, and tail. The head is falciform (hook-shaped) and contains a highly condensed nucleus, with an acrosome located at its anterior end (Fig. 9a`). The midpiece features a helical mitochondrial sheath that surrounds the axoneme and outer dense fibers. The tail, or flagellum, comprises the principal and end pieces, both structured around a central axoneme, which is encased by outer dense fibers and a fibrous sheath (Fig. 9a).

Microscopic examination of epididymal sperm revealed various morphological abnormalities affecting both the

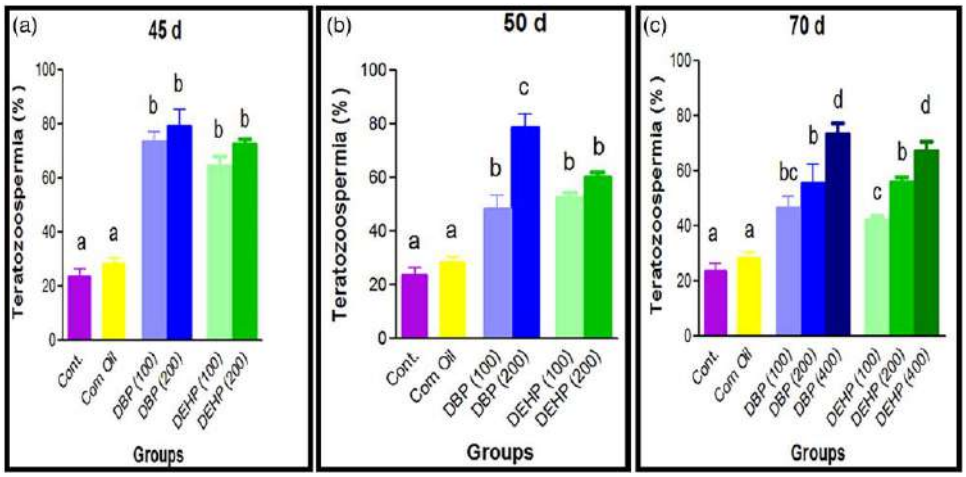


Fig. 8. Teratozoospermia in control, DBP, and DEHP-exposed groups (100, 200, and 400 mg/kg). Different Latin letters indicate significant differences between groups ($p < 0.05$). (**a**) At 45 days of age, (**b**) at 50 days of age, and (**c**) at 70 days of age.

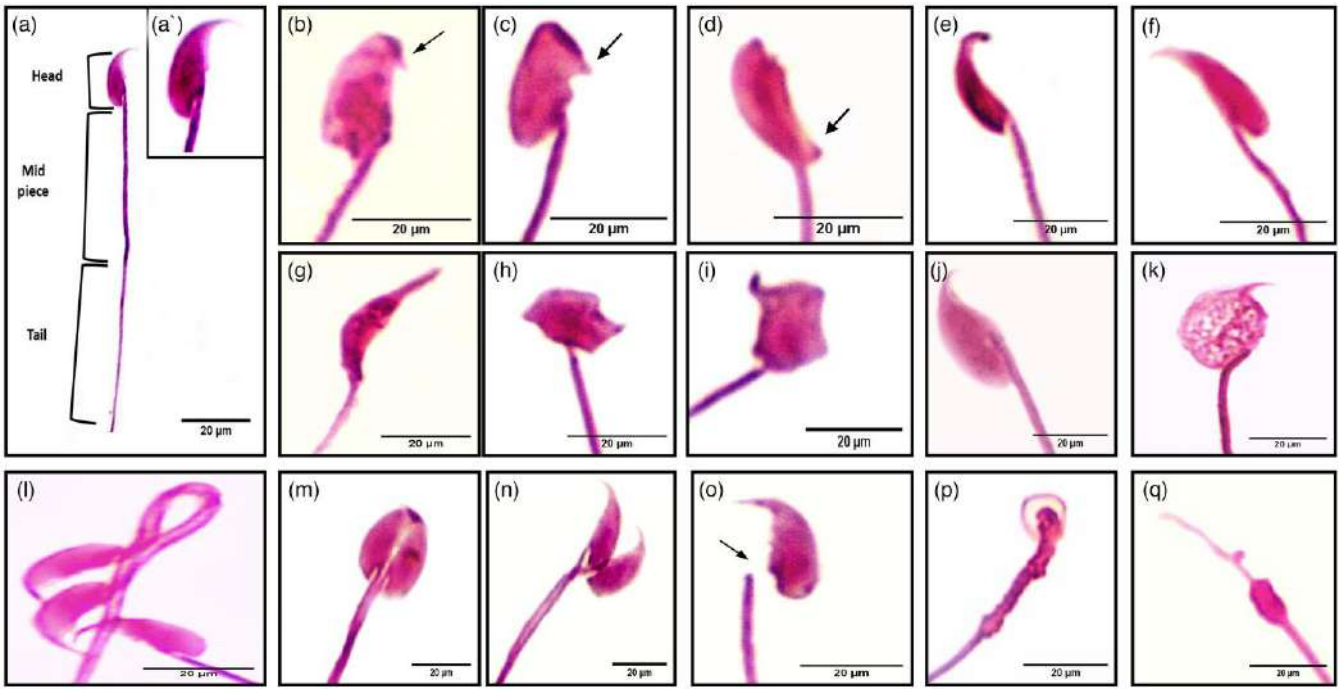


Fig. 9. Photomicrographs illustrating sperm head abnormalities in control and phthalate-treated groups. B = DBP-treated group; E = DEHP-treated group. (**a**) Normal sperm structure showing the principal components. (**a`**) A higher magnification view of the sperm head. Abnormal head morphologies in treated groups include hookless sperm heads. [(**b**) B400, (**c**) E400 and (**d**) E100], banana-shaped sperm head [(**e**) E400, (**f**, **g**) B400], amorphous sperm head [(**h**) B400 and (**i**) E400], large sperm head [(**j**, **k**) E100], double-headed sperm [(**l**) E100, (**m**, **n**) B100], detached sperm head [(**o**) E400], and headless sperm [(**p**) B100 and (**q**) E200]. H and E stain. ×1000.

Downloaded from academic.oup.com/mam/article/32/6/ozag107/8979578 by Ragesh Nair Nair on 17 November 2026

head and tail regions of the spermatozoa. Head defects included hookless heads (Figs. 9a–9c), banana-shaped forms (Figs. 9e–9g), amorphous (Figs. 9h, 9i) and large heads (Figs. 9j, 9k), double-headed sperm (Figs. 9i–9n), detached heads (Fig. 9o), and spermatozoa entirely lacking heads (Figs. 9p, 9q). These abnormalities are suggestive of disturbances in spermiogenesis or chromatin condensation. Midpiece and neck abnormalities were frequently observed and included bent necks (Figs. 10a–10d), folded necks (Figs. 10e–10h), hairpin-like loops (Figs. 10i–10l), and retention of cytoplasmic droplets (Figs. 10m–10q). Tail abnormalities were also common and comprised coiled tails (Figs. 11a–11e), shortened tails (Figs. 11f–11h), and duplicated tails (Figs. 11i–11l). Such morphological abnormalities indicate impaired spermatogenesis and are associated with reduced sperm quality.

Transmission Electron Microscopy

Sertoli Cells

Control group at 36 days of age: under TEM, Sertoli cells appear large and irregularly shaped, with euchromatic oval nuclei and prominent nucleoli. Their cytoplasm extends between developing germ cells and contains abundant mitochondria and smooth endoplasmic reticulum (Fig. 12a) By 50 days of age, the testis is considered functionally mature, with fully differentiated and more elongated Sertoli cells, and spermatogenesis becomes complete (Fig. 12b).

Ultrastructural investigations of testicular tissue in phthalate-treated groups revealed prominent intracellular spaces (Figs. 12c, 12f, 12g, 13e) and multiple cytoplasmic vacuoles within Sertoli and germ cells (Figs. 12e, 12h, 13f–13h, 14e). Intranuclear spaces (Fig. 13d) and necrotic germ cells were also observed (Figs. 13c, 13g), together with increased lipid droplets within Sertoli cells (Figs. 13c, 13d, 13g–13i, 14e). Swollen and vacuolated mitochondria with empty matrices (Figs. 12g, 13f–13h) or degenerated mitochondria (Figs. 12d, 12f, 13e) were frequently detected.

Numerous mitochondria were observed within Sertoli cells, accompanied by dilation and proliferation of smooth (Fig. 12i) and rough endoplasmic reticulum (Figs. 13a, 13b). Sertoli cell nuclei showed irregular contours, distortion, and increased nuclear infolding (Figs. 12f, 13d, 13g). An increased number of peroxisomes were also identified in both Sertoli and germ cells (Figs. 12d, 12h, 13c, 13e–13h). Excessive collagen fiber deposition was observed in the intercellular space, apparently derived from Sertoli cells (Fig. 13b). An increase in the peritubular myoid cell layer surrounding the seminiferous tubules was also evident (Figs. 12g, 13f, 14a–14c). Multinucleated giant cells (MGCs) were observed in the testicular tissue and classified into two types. Multinucleated giant macrophages were located near the lumen of seminiferous tubules and showed irregular morphology, abundant granular cytoplasm with vacuoles, secondary lysosomes, and degenerated mitochondria, along with multiple nuclei of variable size and peripheral or scattered distribution (Fig. 14d). Multinucleated germ cells were observed within seminiferous tubules between germ cells, appearing as large round cells with two or more centrally located uniform nuclei, and showing scant to moderate cytoplasm with few vacuoles and well-defined borders (Fig. 14e). Some germ cells also exhibited autophagic features (Fig. 14f).

Leydig Cells

Control group at 36 days of age: Leydig cells are located in the interstitial tissue and display a polygonal appearance with round or oval nuclei. Their cytoplasm is rich in smooth endoplasmic reticulum, mitochondria with tubular cristae, and

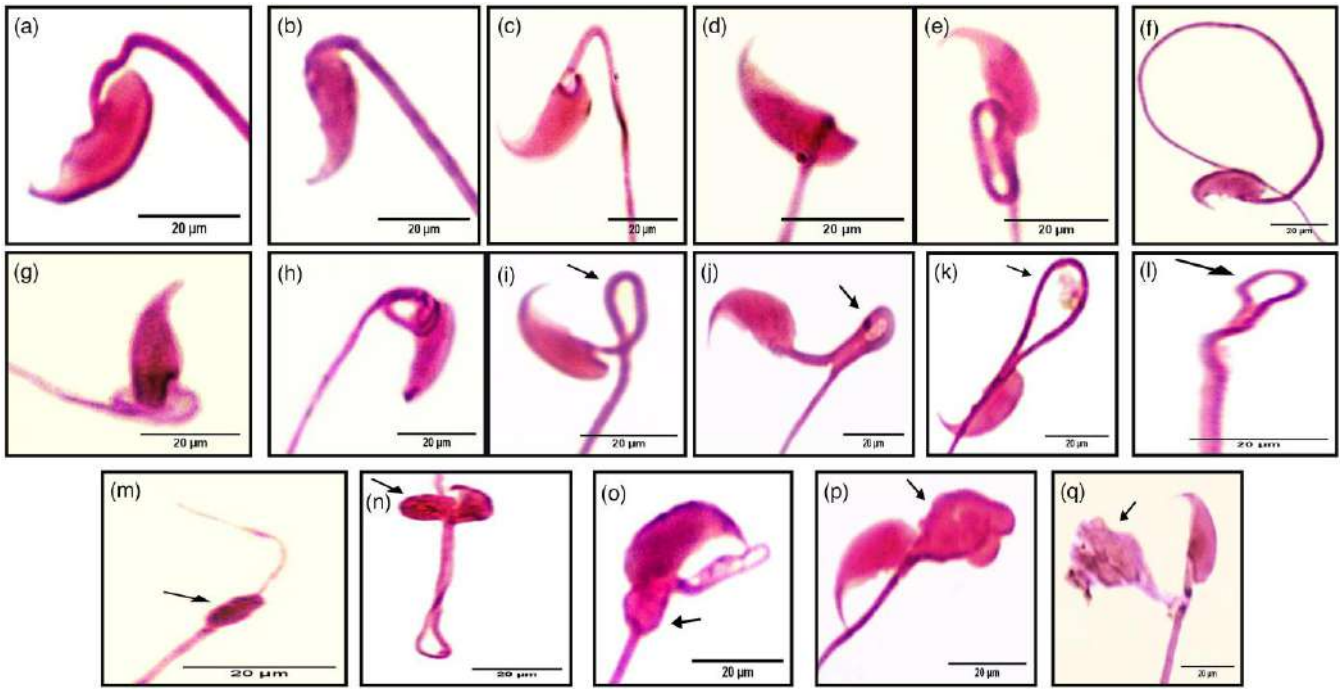


Fig. 10. Photomicrographs illustrating sperm midpiece abnormalities in phthalate-treated groups. Abnormalities include a bent sperm neck [(**a**) E400, (**b**) E400, (**c**) B200, and (**d**) B100], a folded sperm tail [(**e**) E400, (**f**) E400, (**g**) B400, and (**h**) B400], a hairpin-like looped sperm tail [(**i**) E100, (**j**) E100, (**k**) E400, and (**l**) B400], and the presence of a cytoplasmic droplet [(**m**) B400, (**n**) B400, (**o**) E400, (**p**) E100, and (**q**) E200]. H and E stain.×1000.

Downloaded from academic.oup.com/mam/article/32/6/ozag107/8979578 by Ragesh Nair Nair on 17 November 2026

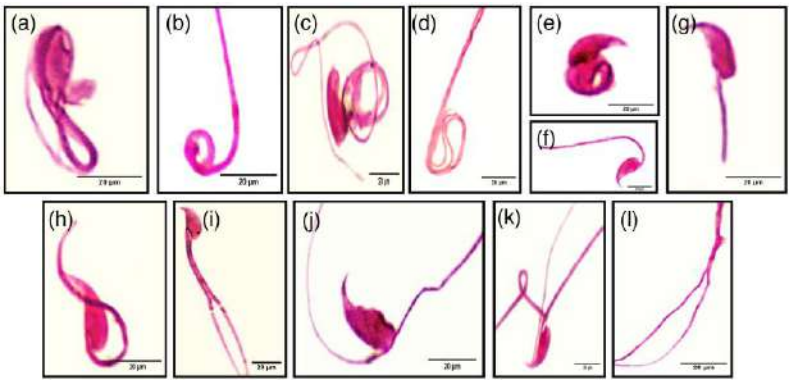


Fig. 11. Photomicrographs illustrating sperm tail abnormalities in phthalate-treated groups. Abnormal tail morphologies include coiled sperm tail [(**a**) E400, (**b**) E400, (**c**) E400, (**d**) B400, and (**e**) B100], shortened sperm tail [(**f**–**h**) E400], and duplicated sperm tail [(**i**) E200, (**j**) E400, (**k**) E100, and (**l**) B100]. H and E stain. ×1000.

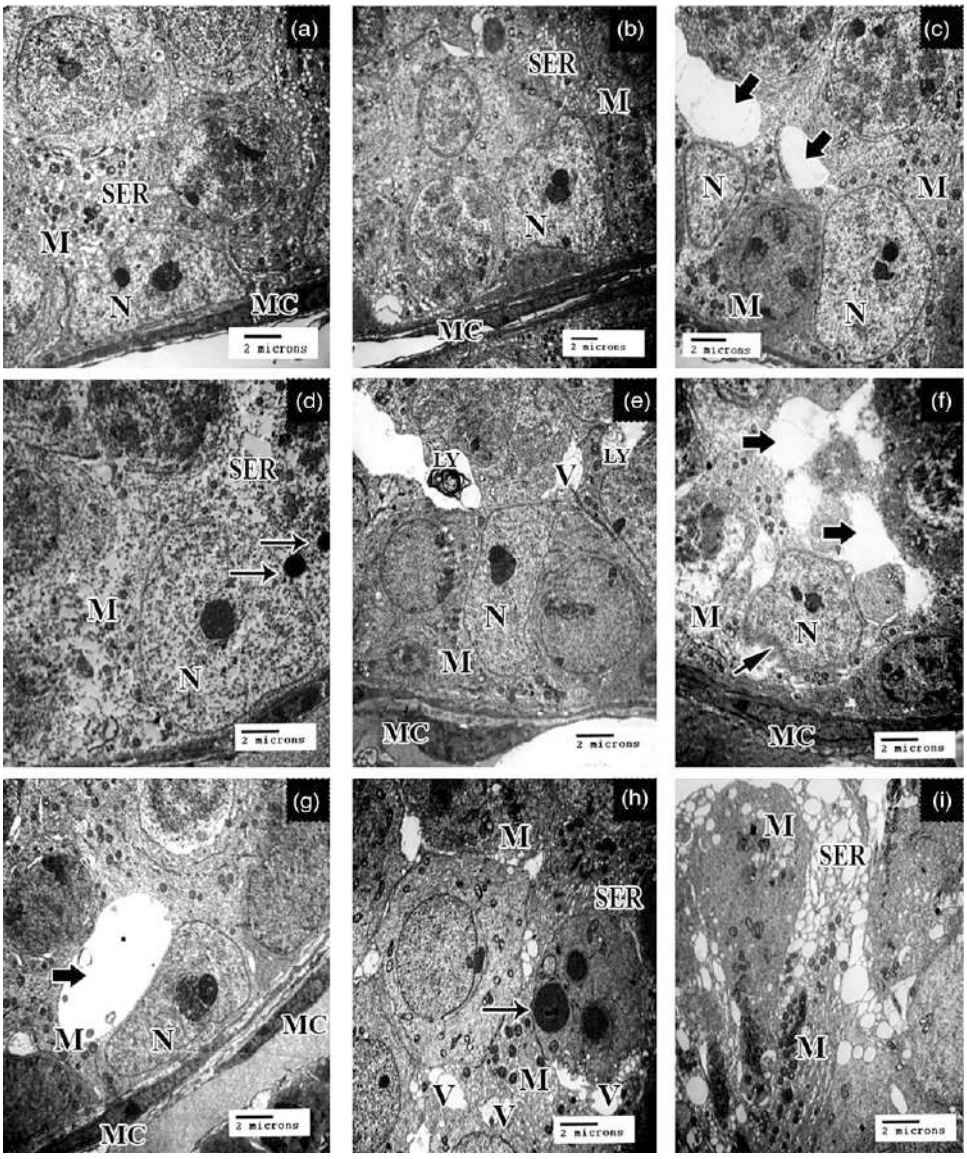


Fig. 12. An electron photomicrograph illustrating ultrastructural changes in Sertoli cells of control and DBP-treated testes at different ages. (**a**) Control at 36 days of age, (**b**) Control at 50 days of age; (**c**) B100 at 36 days of age, (**d**) B100 at 50 days of age; (**e**) B200 at 36 days of age, (**f**) B200 at 50 days of age; (**g**) B400 at 36 days of age, (**h**, **i**) B400 at 50 days of age. N, Sertoli cell nucleus; MC, myoid cell; M, mitochondria; SER, smooth endoplasmic reticulum; V, vacuole; bold arrows, intracellular spaces; short arrows, nuclear envelope infoldings and nuclear distortion; arrows, peroxisomes; arrowhead, lipid droplets; LY, secondary lysosome. ×3600.

Downloaded from academic.oup.com/mam/article/32/6/ozag107/8979578 by Ragesh Nair Nair on 17 November 2026

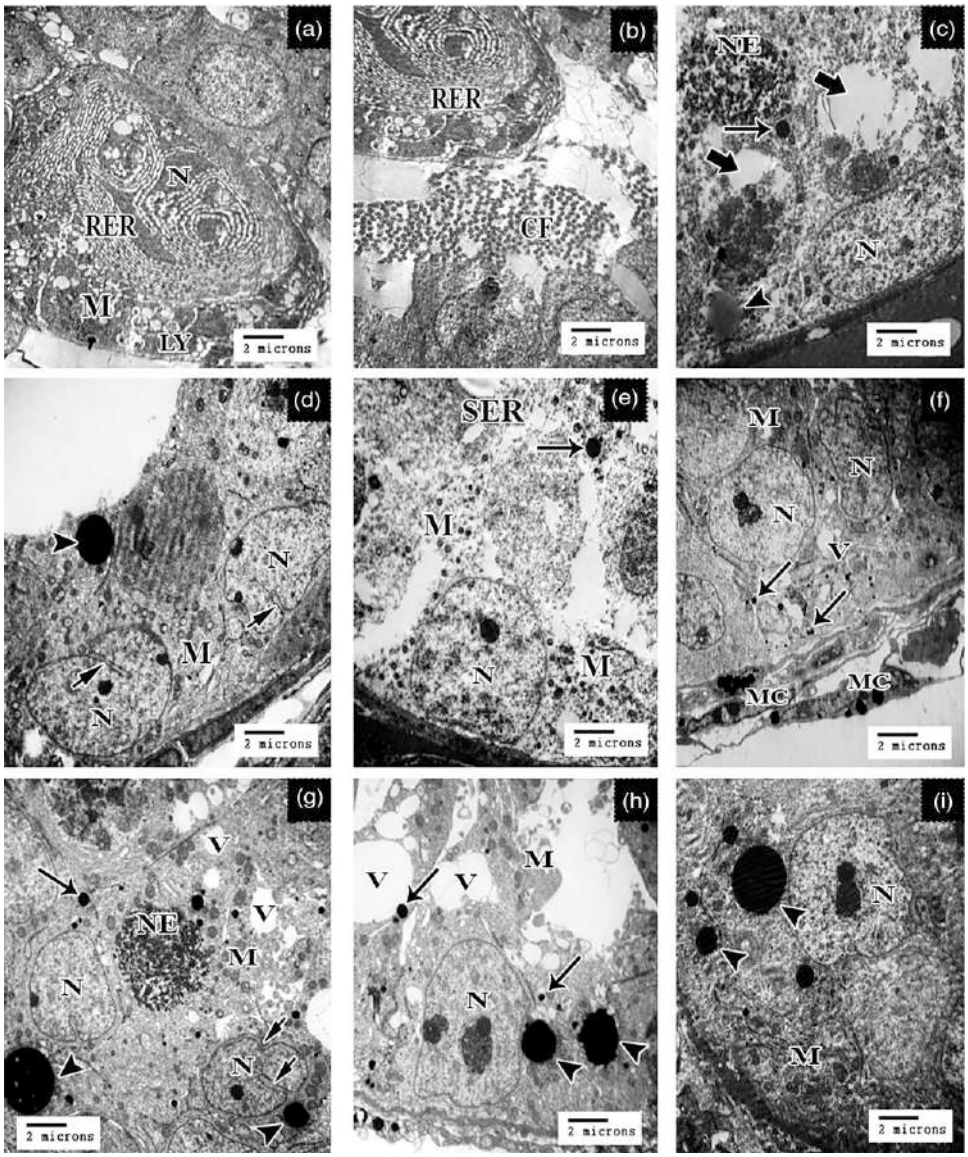


Fig. 13. An electron photomicrograph illustrating ultrastructural changes in Sertoli cells of DEHP-treated testes at different ages. (**a**, **b**) E100 at 36 days of age; (**c**) E100 at 50 days of age; (**d**) E200 at 36 days of age; (**e**) E200 at 50 days of age; (**f**–**h**) E400 at 36 days of age; (**i**) E400 at 50 days of age. N, Sertoli cell nucleus; MC, myoid cell; M, mitochondria; SER, smooth endoplasmic reticulum; RER, rough endoplasmic reticulum; V, vacuole; CF, collagen fibers; bold arrows, intranuclear space; short arrow, nuclear envelope infoldings; arrows, peroxisomes; arrowhead, lipid droplet; NE, necrotic cell; LY, secondary lysosome.×3600.

normally distributed lipid droplets, consistent with active steroidogenesis (Fig. 15a). By 50 days of age, Leydig cells also exhibit full steroidogenic activity (Fig. 15b).

Leydig cells in phthalate groups revealed that massive accumulation of cytoplasmic lipid droplets was apparent (Figs. 15c–15g, 15j, 15k). Numerous mitochondria were concentrated within the cytoplasm (Figs. 14d–14f), and multiple forms of mitochondrial damage were noted. This damage ranged from swollen mitochondria with short or shallow cristae (Fig. 15h) to complete cristae loss (Fig. 15k). Additionally, nuclei showed irregular contours, occasional distortion, and deep indentations (Fig. 15c), as well as infoldings (Fig. 15g). Some cells showed signs of degeneration, including cytoplasmic blebbing and fragmentation, with several membranous vesicles appearing to bud off from the cell (Fig. 15j).

Ultrastructural Quantitative Analysis

For mitochondrial damage in Sertoli cells, two-way ANOVA showed no significant effect of age ($p = 0.7109$) or age × treatment interaction ($p = 0.2801$), but a significant effect of treatment ($p = 0.0008$). This significance was mainly driven by differences between the control and DEHP-treated groups, whereas no significant differences were observed between the control and DBP-treated groups at either age ($p > 0.05$). Mitochondrial damage increased in both DBP and DEHP groups, particularly at 36 days of age in the high-dose groups (400 mg/kg), with values of 37 and 47.90%, respectively, compared with 10.28% in controls, and remained elevated at 50 days of age, mainly in DEHP-treated groups (Fig. 16a).

Sertoli cell vacuolization showed a significant effect of age ($p = 0.0033$) and treatment ($p < 0.0001$), whereas no significant interaction between age and treatment was observed

Downloaded from academic.oup.com/mam/article/32/6/ozag107/8979578 by Ragesh Nair Nair on 17 November 2026

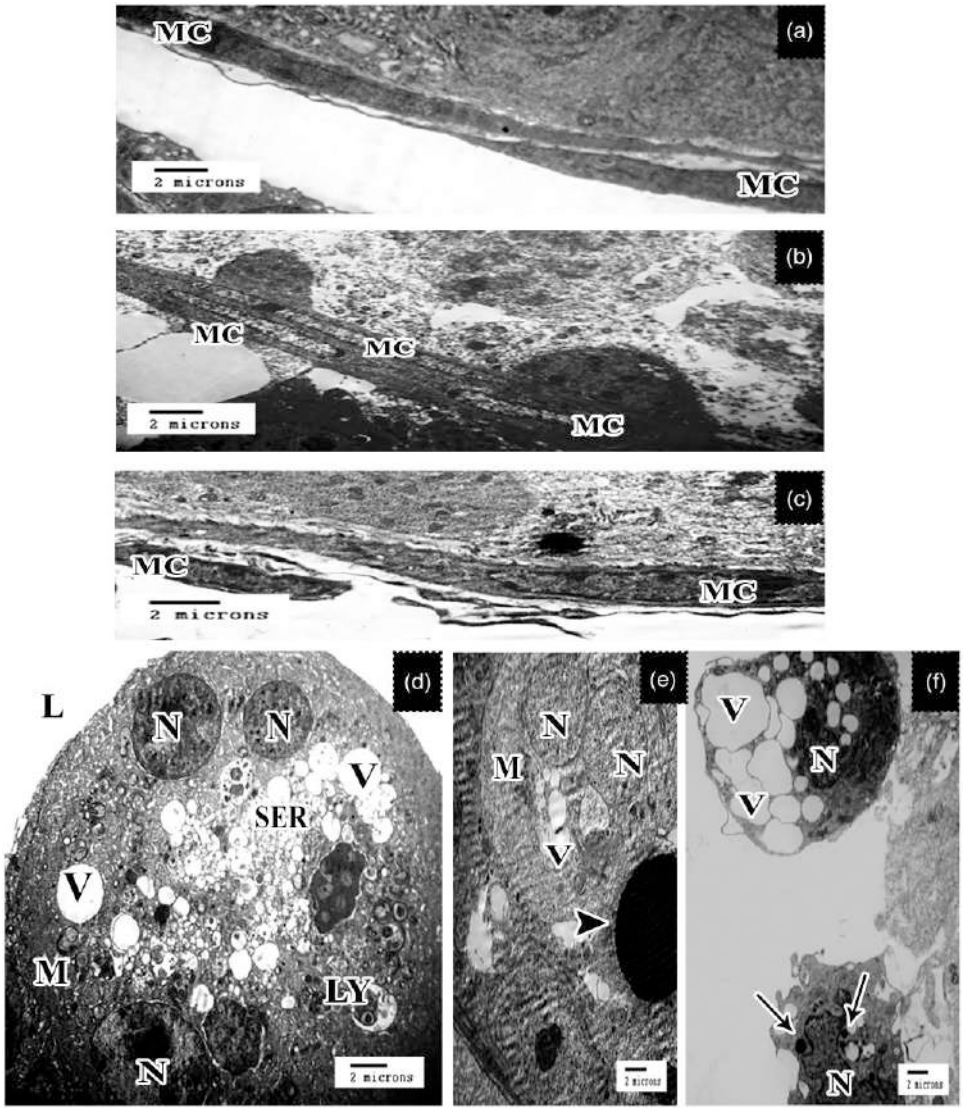


Fig. 14. An electron photomicrograph illustrating ultrastructural changes in treated testes. (**a**–**c**) Increased myoid cell layer: (**a**) E200; (**b**) E100; (**c**) B200. (**d**, **e**) presence of multinucleated giant cells (MGCs) (**d**) B200 at 36 days of age. (**e**) E400 at 50 days of age. ×2900. (**f**) Showing autophagic features in B400 at 36 days of age. MC, myoid cell; N, nucleus; M, mitochondria; SER, smooth endoplasmic reticulum; V, vacuole; L, tubular lumen; arrows, peroxisomes; arrowhead, lipid droplet; LY, secondary lysosome.×3600.

($p = 0.1574$). Vacuolization was absent in control and DBP (100 mg/kg) groups at both ages (0 vacuoles/cell), while higher-dose groups exhibited marked increases, particularly in DBP (200 and 400 mg/kg), reaching a peak value of 8.67 vacuoles/cell in the DBP (400 mg/kg). At 50 days of age, a significant reduction in vacuolization was observed in most treated groups compared with 36 days of age. However, values remained significantly higher than controls in high-dose DBP and DEHP groups (Fig. 16b).

Lipid area fraction in Leydig cells showed significant effects of age, treatment, and their interaction ($p < 0.0001$). A marked increase was observed at 50 days of age compared with 36 days of age, particularly in the DBP (400 mg/kg) group (>50% compared with ~32% at 36 days), indicating no recovery in high-dose DBP. In contrast, DEHP (100 mg/kg) showed a significant reduction at 50 days (~2.4% compared with ~8.2% at 36 days of age), whereas DEHP (200 mg/kg) remained elevated (~18–19% at both ages) compared with controls (~6%) (Fig. 16c).

Immunohistochemical Expression of Inhibin-α, Calretinin and PPAR-γ

At 36 Days of Age

Inhibin-*α*. The control group exhibited clear expression of inhibin-*α* in Sertoli cells (Fig. 17a), whereas treated groups showed markedly reduced staining intensity (Figs. 17b, 17c, 17e, 17g). Interestingly, contrary to expectations, the high dose of DBP (400 mg/kg) (Fig. 17d) and the medium dose of DEHP (200 mg/kg) (Fig. 17f) demonstrated stronger Inhibin-*α* expression. OD analysis also revealed a statistically significant decrease in staining intensity in all treated groups compared with the control, except for the high dose of DBP and the medium dose of DEHP, which showed a significant increase in expression ($p < 0.0001$; $F(6,63) = 6.682$; $\eta p^2 = 0.39$; Fig. 17h).

Calretinin. Calretinin expression was strong and clearly observed in Leydig cells of the control group (Fig. 18a), whereas

Downloaded from academic.oup.com/mam/article/32/6/ozag107/8979578 by Ragesh Nair Nair on 17 November 2026

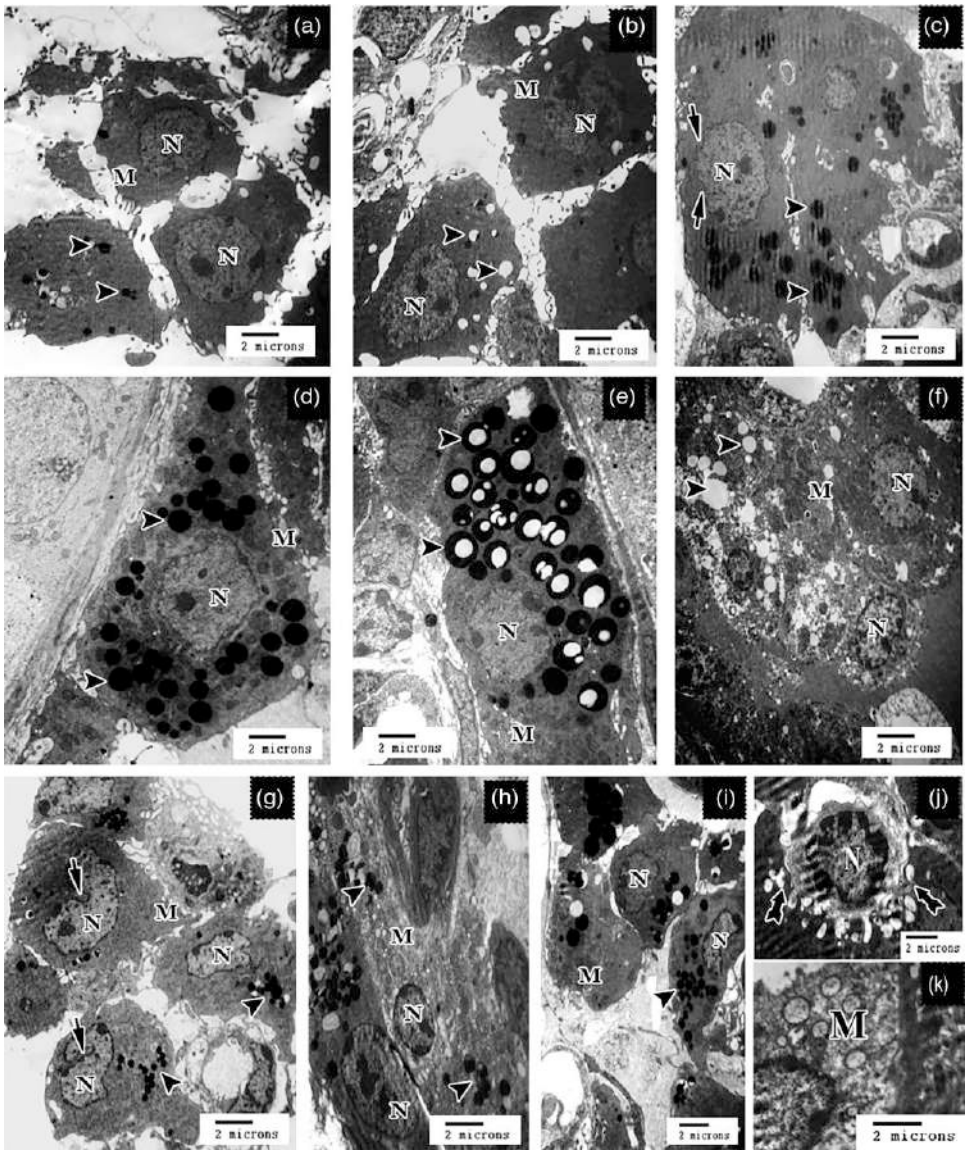


Fig. 15. An electron photomicrograph of Leydig cells in control and treated testes at different ages. (**a**) Control at 36 days of age; (**b**) Control at 50 days of age; (**c**) B100 at 50 days of age; (**d**, **e**) B400 at 50 days of age; (**f**) E200 at 50 days of age; (**g**) E400 at 36 days of age; (**h**) E400 at 50 days of age; (**i**) E200 at 36 days of age, and (**j**, **k**) E400 at 50 days of age. N, Leydig nucleus; M, mitochondria; arrowhead, lipid droplets; short arrow, nuclear envelope infoldings; Feathered arrow, cytoplasmic blebbing. ×2900.

treated groups generally showed reduced staining intensity (Figs. 18b–18e, 18g), except for the medium dose of DEHP (200 mg/kg) (Fig. 18f), which exhibited pronounced stainability in Leydig cells. Statistical analysis of OD showed a significant decrease in staining intensity in all treated groups compared with control, whereas the medium dose exhibited a significant increase compared with both control and other treated groups ($p < 0.0001$; $F(6,63) = 16.27$; $\eta p^2 = 0.61$; Fig. 18h).

Peroxisome Proliferator Activating Receptor Gamma. Peroxisome proliferator activating receptor gamma (PPAR-γ) expression was very weak in Leydig and Sertoli cells of the control group (Fig. 19a), whereas treated groups exhibited strong stainability in Leydig cells (Figs. 19b, 19d, 19f). In Sertoli cells, some staining was observed in the medium dose of DBP (200 mg/kg) (Fig. 19c) and the low and high doses of DEHP (100 and 400 mg/kg) (Fig. 19e, 19g). Statistical analysis of OD showed a significant increase in PPAR-γ staining intensity in treated groups compared with the control, with the medium dose of DEHP exhibiting the highest increase ($p < 0.0001$; $F(6,63) = 15.67$; $\eta p^2 = 0.60$; Fig. 19h).

At 70 Days of Age

Inhibin-α. Inhibin-α expression in Sertoli cells was regular and clearly observed among germ cells in the control group (Fig. 20a), whereas the lowest dose of DBP (100 mg/kg) exhibited disrupted staining (Fig. 20b), while all other groups showed consistently reduced expression intensity (Figs. 20c–20g). Statistical analysis of OD revealed a significant decrease in staining intensity in all treated groups compared with the control, with the lowest expression observed in the groups receiving the highest doses of both compounds ($p < 0.0001$; $F(6,63) = 7.934$; $\eta p^2 = 0.43$; Fig. 20h).

Downloaded from academic.oup.com/mam/article/32/6/ozag107/8979578 by Ragesh Nair Nair on 17 November 2026

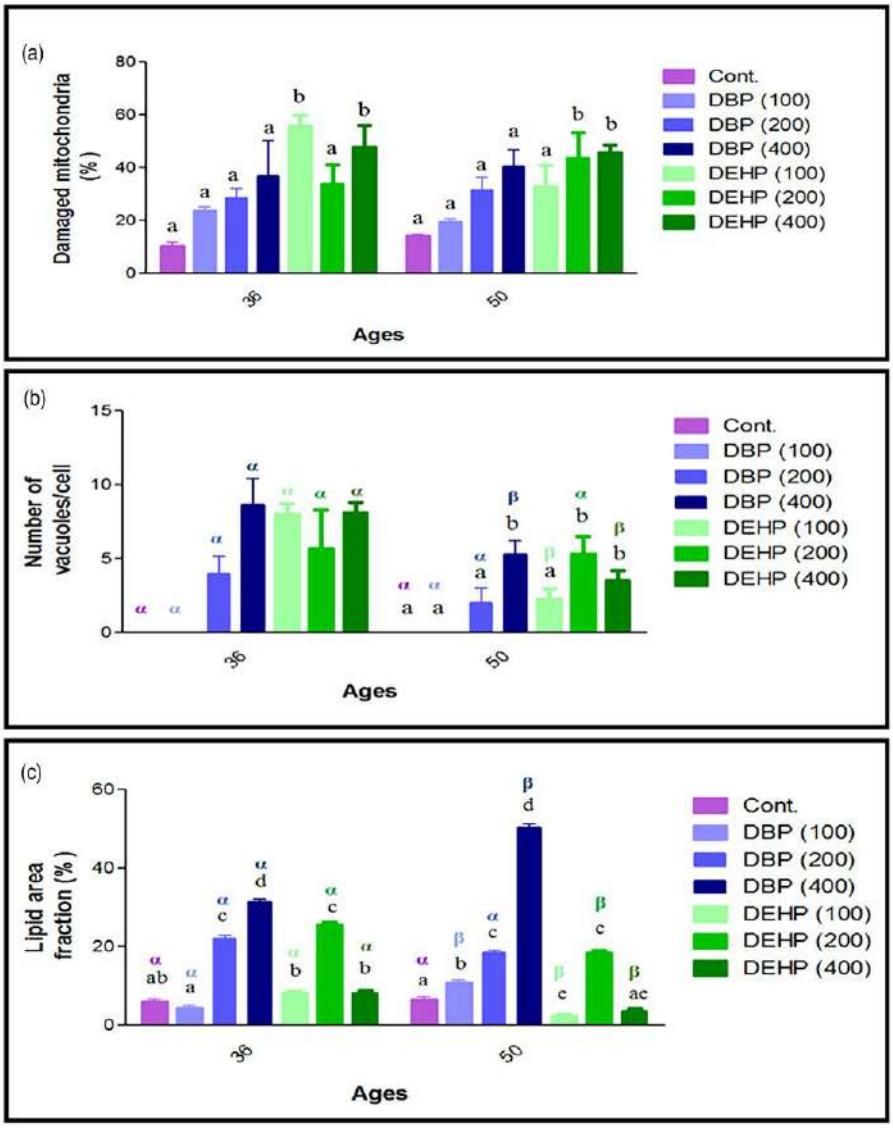


Fig. 16. Ultrastructural quantitative analysis at 36 and 50 days showing (**a**) damaged Sertoli cell mitochondria (%), (**b**) Sertoli cell vacuolization (vacuoles/cell), and (**c**) Leydig cell lipid area fraction (%). Different Latin letters denote significant differences between groups, while Greek letters indicate significant differences between developmental ages ($p < 0.05$).

Calretinin. Calretinin expression was observed in Leydig cells of the control group (Fig. 21a), whereas treated groups generally exhibited reduced staining across all treatments (Figs. 21b, 21c, 21e, 21g). Notably, the high dose of DBP (400 mg/kg) and the medium dose of DEHP (200 mg/kg) demonstrated relatively stronger expression (Figs. 21d, 21f). Statistical analysis of OD revealed a significant decrease in staining intensity in treated groups compared with the control, whereas the medium dose of DEHP and the high dose of DBP showed a significant increase compared with the control ($p < 0.0001$; $F(6,63) = 20.9$; $\eta p^2 = 0.67$; Fig. 21h).

Peroxisome Proliferator Activating Receptor Gamma

PPAR-γ expression was faintly observed in Leydig and Sertoli cells of the control group (Fig. 22a). In treated groups, staining was stronger overall, with DEHP-treated groups (Figs. 22e–22g) showing more pronounced expression compared with DBP-treated groups (Figs. 22b–22d). Statistical analysis revealed a significant increase in PPAR-γ staining intensity in all treated groups compared with the control, with DEHP-treated groups showing a significantly stronger increase than DBP-treated groups ($p < 0.0001$; $F(6,63) = 5.356$; $\eta p^2 = 0.34$; Fig. 22h).

Two-way ANOVA showed no significant effect of age or age × treatment interaction for inhibin-α, calretinin, or PPAR-γ expression ($p > 0.05$).

Discussion

Exposure to phthalates during critical periods of development represents a significant concern for male reproductive dysfunction. In the present study, exposure to DBP and DEHP in immature mice resulted in dose-dependent alterations in body and testicular weights, marked deterioration of sperm parameters, and profound ultrastructural changes within testicular tissue. These functional impairments were accompanied by altered

Downloaded from academic.oup.com/mam/article/32/6/ozag107/8979578 by Ragesh Nair Nair on 17 November 2026

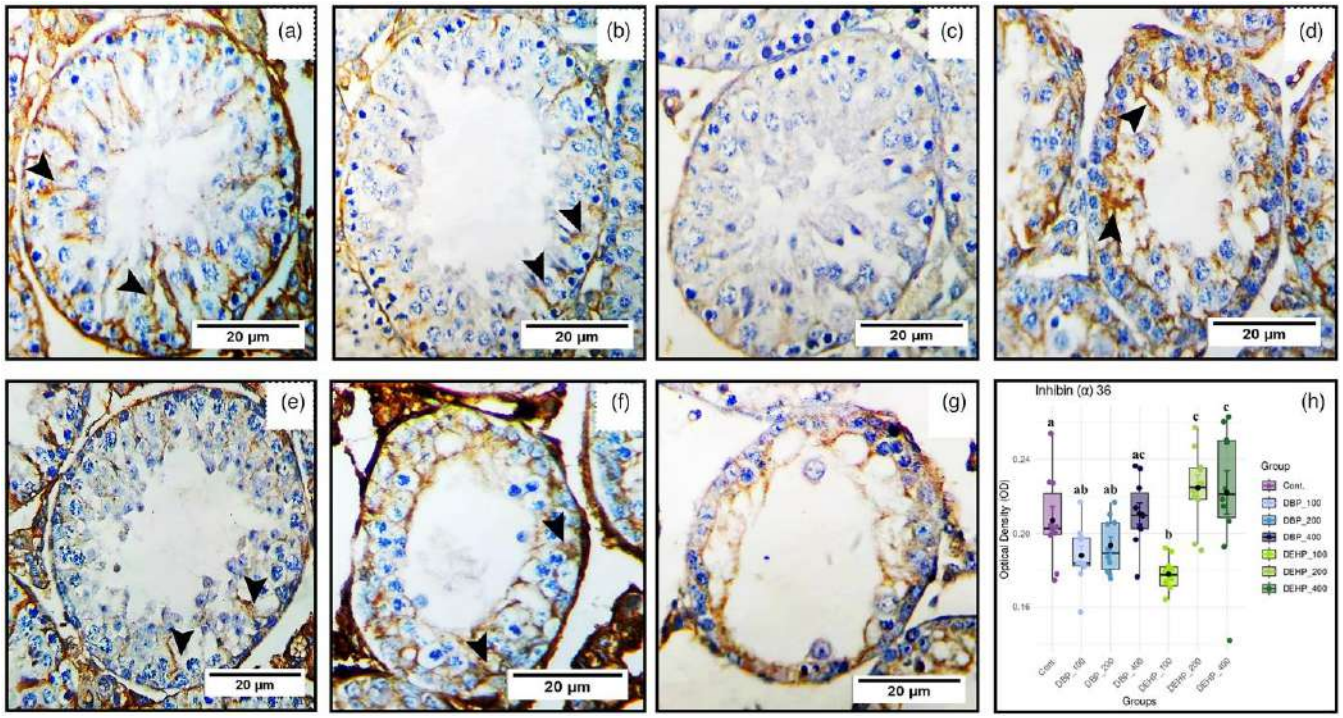


Fig. 17. Immunohistochemical detection of inhibin-α in testicular tissue at 36 days of age. Representative micrographs: (**a**) Control, (**b**) B100, (**c**) B200, (**d**) B400, (**e**) E100, (**f**) E200, and (**g**) E400. Sertoli cells (arrowheads). ×400. (**h**) Optical density (OD) measurements. Different Latin letters denote significant differences between groups ($p < 0.05$).

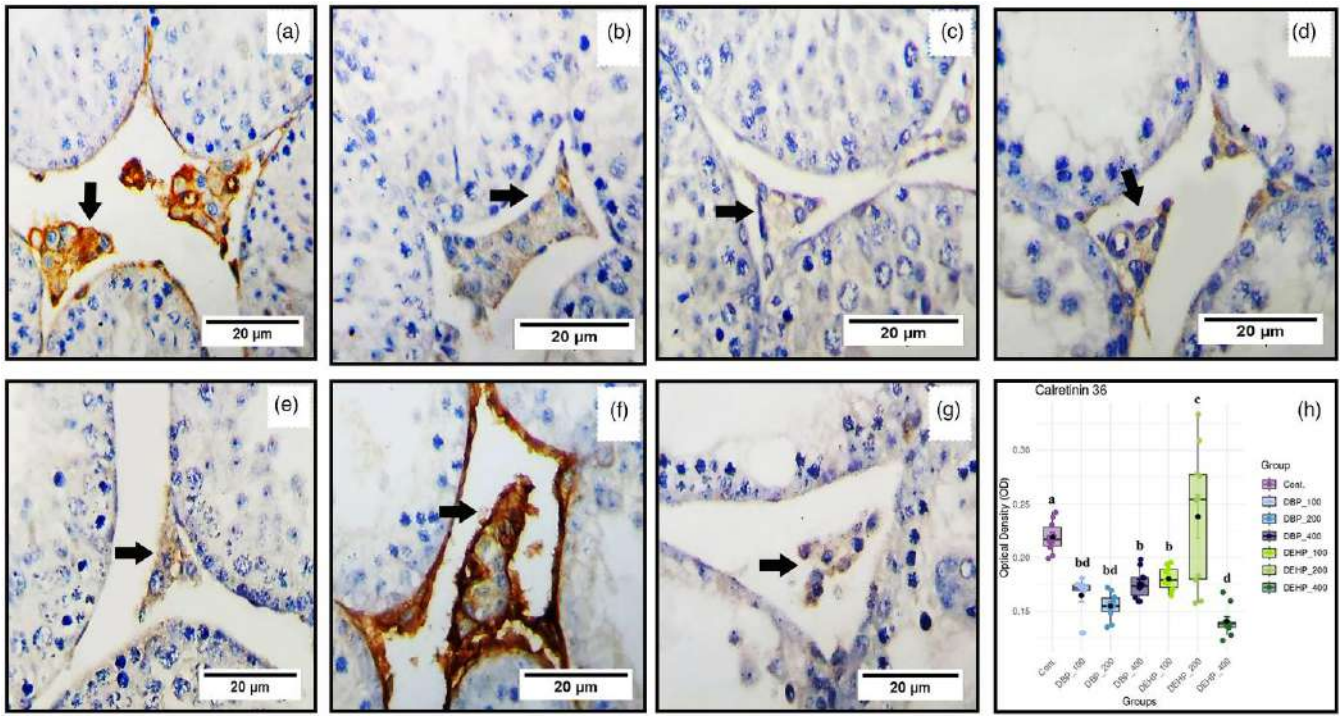


Fig. 18. Immunohistochemical detection of calretinin in testicular tissue at 36 days of age. Representative micrographs: (**a**) Control, (**b**) B100, (**c**) B200, (**d**) B400, (**e**) E100, (**f**) E200, and (**g**) E400. Leydig cells (thick arrows). ×400. (**h**) Optical density (OD) measurements. Different Latin letters denote significant differences between groups ($p < 0.05$).

immunoexpression of key regulators implicated in steroidogenesis and seminiferous epithelial homeostasis. The integration of morphometric, ultrastructural, and immunohistochemical findings suggests that phthalate exposure compromises testicular integrity through coordinated disturbances in metabolic regulation, cellular architecture, and spermatogenic progression.

Downloaded from academic.oup.com/mam/article/32/6/ozag107/8979578 by Ragesh Nair Nair on 17 November 2026

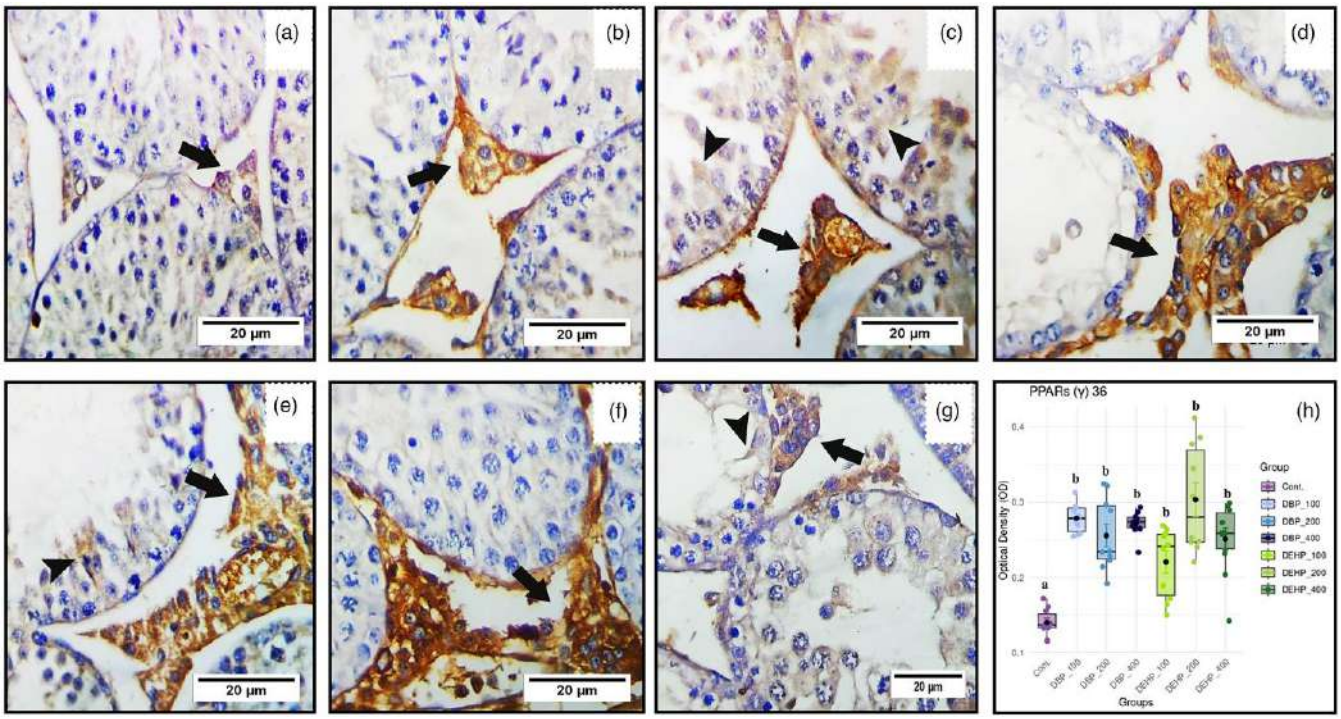


Fig. 19. Immunohistochemical detection of PPAR-γ in testicular tissue at 36 days of age. Representative micrographs: (**a**) Control, (**b**) B100, (**c**) B200, (**d**) B400, (**e**) E100, (**f**) E200, and (**g**) E400. Leydig cells (thick arrows) and Sertoli cells (arrowheads). ×400. (**h**) Optical density (OD) measurements. Different Latin letters denote significant differences between groups ($p < 0.05$).

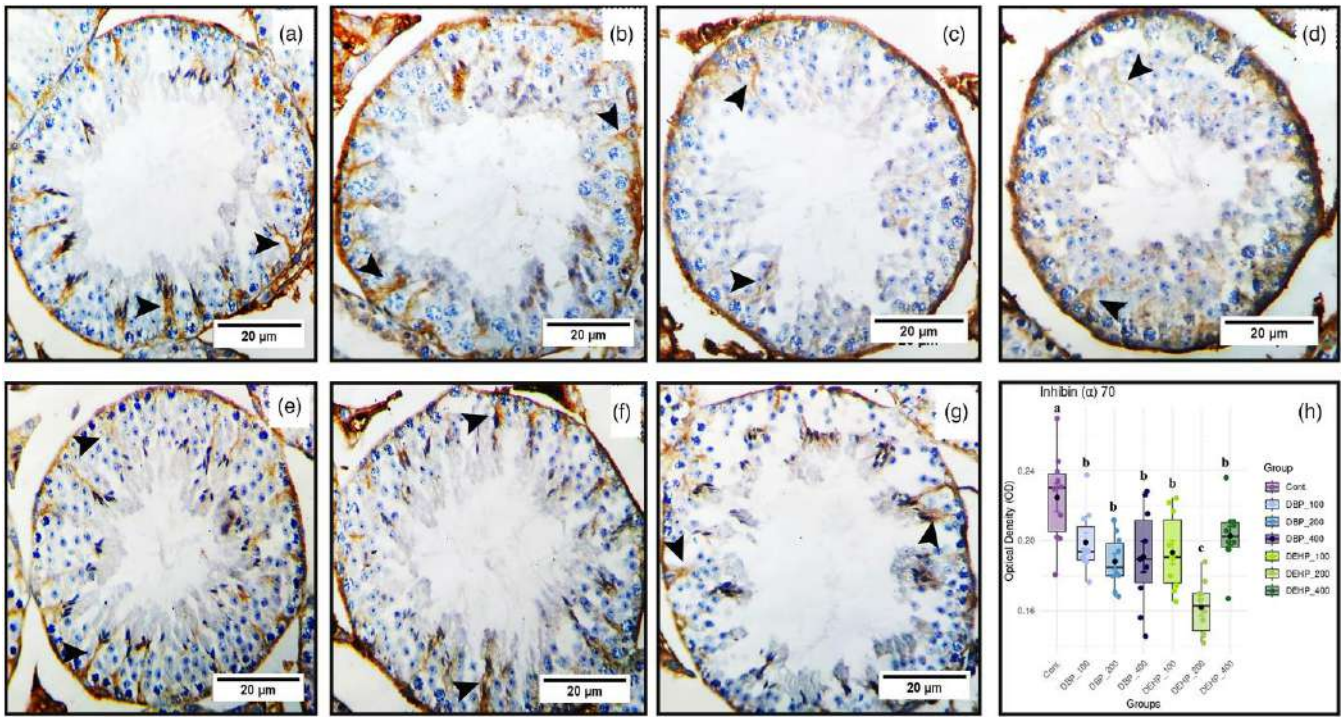


Fig. 20. Immunohistochemical detection of inhibin-α in testicular tissue at 70 days of age. Representative micrographs: (**a**) Control, (**b**) B100, (**c**) B200, (**d**) B400, (**e**) E100, (**f**) E200, and (**g**) E400. Sertoli cells (arrowheads). ×400. (**h**) Optical density (OD) measurements. Different Latin letters denote significant differences between groups ($p < 0.05$).

Although partial recovery was observed at later developmental stages, particularly in low-dose groups, several ultrastructural and immunohistochemical alterations persisted, indicating incomplete restoration of testicular function. Although these doses exceed typical environmental human exposure levels (Eslami et al., 2025), high-dose animal models are widely

Downloaded from academic.oup.com/mam/article/32/6/ozag107/8979578 by Ragesh Nair Nair on 17 November 2026

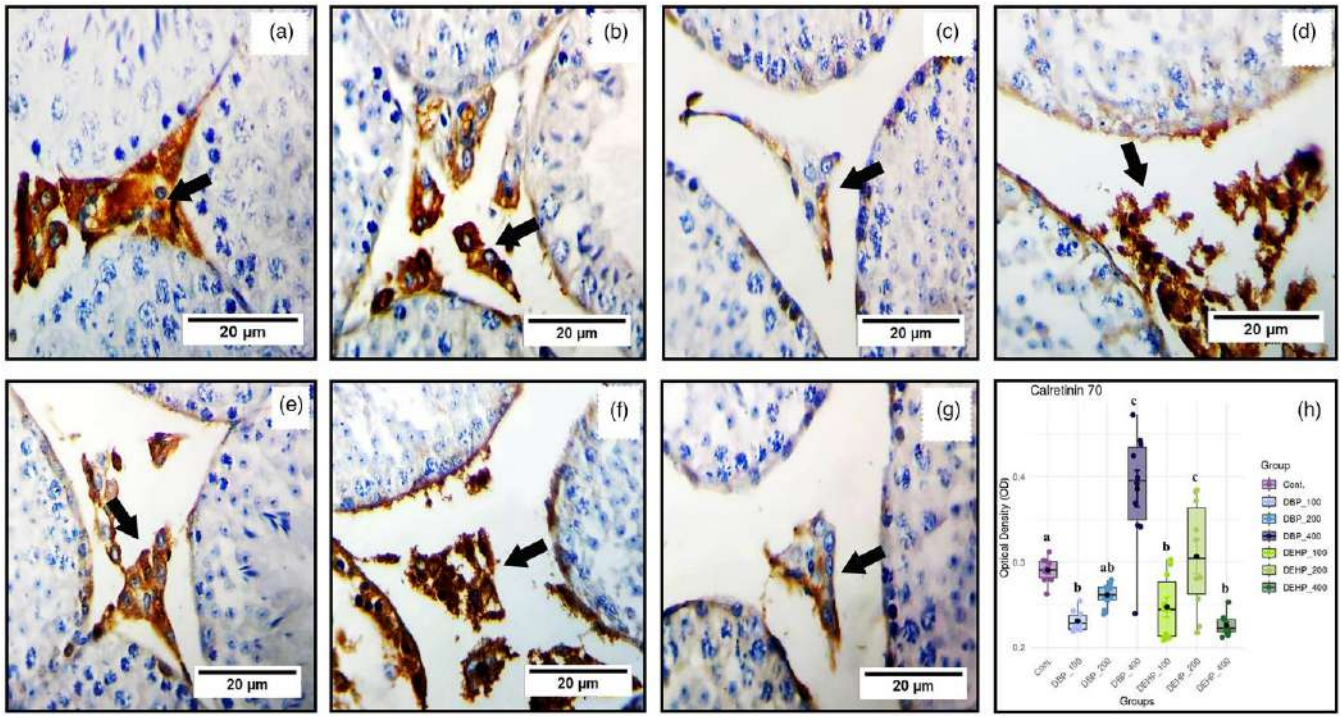


Fig. 21. Immunohistochemical detection of calretinin in testicular tissue at 70 days of age. Representative micrographs: (**a**) Control, (**b**) B100, (**c**) B200, (**d**) B400, (**e**) E100, (**f**) E200, and (**g**) E400. Leydig cells (thick arrows). ×400. (**h**) Optical density (OD) measurements. Different Latin letters denote significant differences between groups ($p < 0.05$).

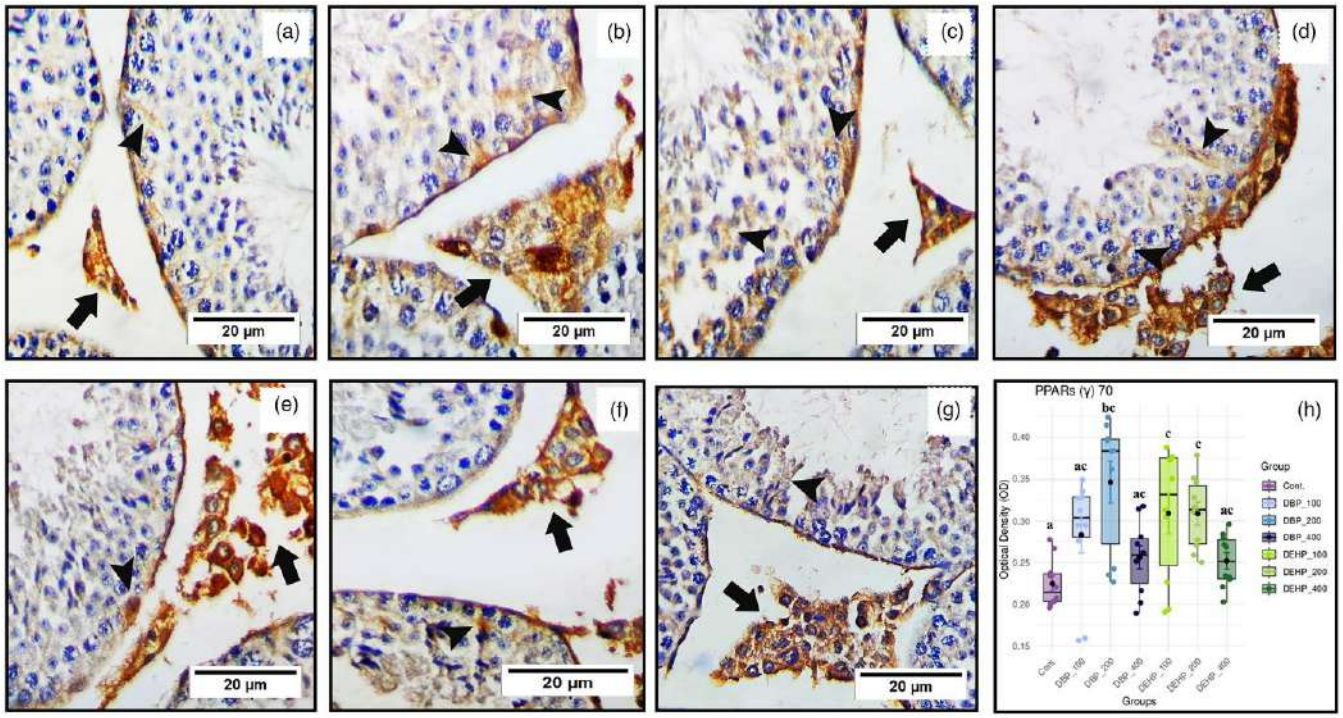


Fig. 22. Immunohistochemical detection of PPAR-γ in testicular tissue at 70 days of age. Representative micrographs: (**a**) Control, (**b**) B100, (**c**) B200, (**d**) B400, (**e**) E100, (**f**) E200, and (**g**) E400. Leydig cells (thick arrows) and Sertoli cells (arrowheads). ×400. (**h**) Optical density (OD) measurements. Different Latin letters denote significant differences between groups ($p < 0.05$).

employed to identify toxicological hazards and characterize dose-dependent mechanisms that may also operate during chronic low-level exposure (Wang et al., 2021; Reddy et al., 2025).

In this study, treatment with both DBP and DEHP significantly affected body and testicular weight in male mice. While DBP exposure caused a decrease in body weight, DEHP-treated mice, unexpectedly, showed a marked increase.

Downloaded from academic.oup.com/mam/article/32/6/ozag107/8979578 by Ragesh Nair Nair on 17 November 2026

This may be related to differences in how each compound interferes with metabolic regulation and gut microbiota composition. DEHP exposure has been shown to induce gut dysbiosis, characterized by an increased Firmicutes/Bacteroidetes ratio and reduced beneficial bacteria such as *Lactobacillus* and *Bifidobacterium* (Lei et al., 2019; Tian et al., 2019; Fu et al., 2021). In addition to altering microbial composition, DEHP also disrupts microbial metabolic activity, leading to changes in gut-derived metabolites involved in host energy metabolism (Lei et al., 2019). These alterations enhance energy harvest from the diet, promote lipid accumulation, and impair metabolic homeostasis (Chiu et al., 2020). Furthermore, dysbiosis increases intestinal permeability, allowing endotoxins such as lipopolysaccharide to enter the circulation and trigger chronic low-grade inflammation, which activates adipogenic pathways including PPAR-γ signaling and disrupts lipid metabolism (Tian et al., 2019; Su et al., 2022; Chai et al., 2023; Mostafavi Abdolmaleky & Zhou, 2024). Collectively, these microbiota-mediated metabolic disturbances may explain the atypical body weight gain observed in DEHP-treated mice, suggesting that the increased body weight likely reflects enhanced adipose tissue deposition and metabolic dysregulation. Conversely, the hepatotoxic and metabolic effects of DBP may contribute to weight loss. The reduction in testicular weight observed in both DBP- and DEHP-treated mice suggests testicular atrophy, which may be associated with impaired steroidogenesis and germ cell depletion. These mechanisms are commonly associated with phthalate exposure and will be discussed in detail in the following sections, which address spermatogenic alterations.

The higher mortality observed in DBP-treated groups compared with DEHP may be due to its faster absorption and metabolism (Isobe et al., 2023), leading to more rapid systemic exposure. DBP also induces oxidative stress and activates inflammatory pathways (e.g., NF-κB, IL-6, and TNF-α) (Wang et al., 2020). These combined effects likely contribute to multiorgan dysfunction and increased risk of death, as supported by experimental and epidemiological studies (Beyer et al., 2022). In the present study, the observed mortality (28%) was confined to the high-dose groups and showed a clear dose-dependent pattern, suggesting a treatment-related toxicological effect associated with repeated daily exposure for 15 consecutive days. This interpretation is supported by the well-documented higher acute toxicity of DBP compared with DEHP in rodents. Reported oral LD_{50} values are ~6,300 mg/kg for DBP (European Chemicals Agency (ECHA), 2023) and 30,000–34,000 mg/kg for DEHP (Agency for Toxic Substances and Disease Registry (ATSDR), 2022), indicating a substantially higher intrinsic toxicity of DBP. Accordingly, the observed mortality is considered a dose-dependent, treatment-related outcome consistent with repeated-dose toxicity reported in rodents (National Toxicology Program (NTP), 2021). These findings suggest that increased mortality may be attributed to rapid systemic exposure, oxidative stress, and inflammatory responses resulting in multiorgan dysfunction.

It is believed that phthalates disrupt the male reproductive system. Herein, the study provides compelling evidence that DBP and DEHP exposure exerts significant reproductive toxicity in male mice, primarily by impairing spermatogenesis and disrupting hormonal homeostasis. A marked, dose-dependent, and persistent reduction in sperm concentration was observed in all treated groups, with the highest doses (200 and 400 mg/kg) producing the most pronounced suppression. Although partial recovery of sperm count was noted over time at the lower dose (100 mg/kg), values never reached control levels. This indicates persistent testicular dysfunction and the inability of spermatogenic cells to acclimate to phthalate-induced toxicity during prolonged exposure. Several studies have linked the effects of phthalates on semen parameters to the generation of reactive oxygen species (ROS) at a cellular level. Effects include increased lipid peroxidation, disrupted cell function, and altered expression and activity of the most important antioxidant enzymes. This leads to testicular tissue damage, germ cell apoptosis, and reduced spermatogenesis (Emojevwe et al., 2022). These results, collectively, are in agreement with previous reports and suggest that oxidative stress-mediated damage to germ cells plays a central role in the persistent suppression of spermatogenesis following phthalate exposure. In addition to quantitative reductions, sperm quality was severely compromised, as evidenced by a significant decline in motility and viability, particularly at higher doses. DBP and DEHP at (200 and 400 mg/kg) caused the most pronounced impairment, with many spermatozoa exhibiting sluggish or absent forward progression, correlating with the observed structural abnormalities. At the highest dose (400 mg/kg), exposure exerted a potent spermicidal effect, completely abolishing spermatogenesis for ~35 days after cessation of dosing. Sperm production subsequently reappeared; however, sperm concentration remained markedly reduced, with low viability (≈20%) and severe teratozoospermia (>80%), indicating reinitiation of spermatogenesis in the absence of functional recovery. These findings indicate severe impairment of sperm quality and suggest a substantially reduced reproductive potential following phthalate exposure. Sperm morphological defects, including head and tail abnormalities, are indicative of disrupted spermiogenesis, mitochondrial dysfunction, and epididymal maturation failure. Importantly, recent studies showed that phthalates can bind to receptors on human sperm cells, leading to functional alterations such as ROS overproduction, DNA fragmentation, premature acrosome reactions, elevated caspase activity, and reduced responsiveness to progesterone (Virant-Klun et al., 2022). These alterations likely result from mitochondrial dysfunction, oxidative stress, disrupted spermatogenesis, and failed epididymal maturation, indicating a potent and potentially long-lasting impact on male fertility.

The ultrastructural abnormalities observed provide mechanistic insight into the spermatogenic impairment. Electron microscopy in the present work revealed a marked accumulation of lipid droplets within Leydig cells, accompanied by an increased density of mitochondria. Quantitative analysis further demonstrated a significant increase in lipid area fraction, particularly in the DBP-treated groups, where lipid accumulation exceeded 50% in the high-dose groups. Such coexistence of lipid storage and mitochondrial proliferation is not indicative of efficient steroidogenesis, but rather of a compensatory response. As suggested previously, excessive lipid accumulation reflects impaired trafficking of cholesterol into mitochondria via the StAR protein and defective conversion into pregnenolone, the first step of steroidogenesis (Dees et al., 2001). In agreement, suppression of key steroidogenic genes and proteins by phthalate has been reported (Li & Spade, 2021), reinforcing the current findings. In this context, additionally, ultrastructural examination revealed an increase in the size and dilation of the smooth endoplasmic reticulum,

Downloaded from academic.oup.com/mam/article/32/6/ozag107/8979578 by Ragesh Nair Nair on 17 November 2026

accompanied by numerous swollen mitochondria and evident cytoplasmic vacuolations. Quantitative analysis further confirmed extensive ultrastructural damage, where mitochondrial degeneration reached 37% in the DBP 400 mg/kg group and 47.9% in the DEHP 400 mg/kg group. In parallel, Sertoli cell vacuolization markedly increased in the high-dose groups, averaging ~8 and 5 vacuoles/cell in DBP 400 and DEHP 400 mg/kg groups, respectively. These alterations are consistent with cellular stress and organelle dysfunction induced by toxicant exposure. Recent studies demonstrated that toxicants can induce endoplasmic reticulum stress accompanied by marked morphological alterations (Abd-Elmawla et al., 2026), including dilation of the smooth endoplasmic reticulum (Hassanin et al., 2024). Therefore, the observed expansion of the endoplasmic reticulum may reflect activation of detoxification and stress-response pathways.

It can be suggested that the expansion of the endoplasmic reticulum is due to the activation of detoxification and stress pathways. In the current study, ultrastructural examination revealed a marked proliferation of the rough endoplasmic reticulum in Sertoli cells. This was accompanied by increased secretion of collagen fibers into the intercellular space. It is suggested that Sertoli cells exhibit increased synthetic activity in response to exposure to phthalates. Concurrent detection of collagen fibers and phenotypic changes in Sertoli and peritubular myoid cells indicates early fibrotic remodeling of the seminiferous epithelium. It can be proposed that these phenotypic alterations represent a pathological attempt to repair chronic injury, potentially leading to increased extracellular matrix (ECM) deposition and distortion of seminiferous tubule architecture. These interpretations are in agreement with previous studies reporting alterations in Sertoli and myoid cells. These changes are associated with thickening of the peritubular lamina propria and upregulation of ECM components, including collagen type IV and molecular chaperones such as heat shock protein 47, during early testicular damage (Seco Rovira et al., 2025). Although cryptorchidism in boars has been studied previously (Seco Rovira et al., 2025), the present findings suggest that the observed phenotypic alterations in Sertoli and peritubular myoid cells may be a result of fibroblast-like transformation. This transformation is proposed to occur in response to chronic stress.

Previous studies have demonstrated that testicular cells exposed to phthalates commonly exhibit a dual response involving both autophagy and apoptosis. Initially, autophagy is activated as a cytoprotective mechanism to maintain cellular homeostasis; however, with the persistence of mitochondrial injury and oxidative stress, this adaptive process eventually shifts toward apoptotic cell death (Chen et al., 2025). In the current study, the affected cells displayed numerous cytoplasmic and autophagic vacuoles; swollen or disrupted mitochondria with shallow cristae; and shrunken or pyknotic nuclei. These features are consistent with both autophagic and apoptotic degeneration. Taken together, these findings suggest that mitochondrial damage plays a pivotal role in the transition from autophagy to apoptosis under phthalate-induced oxidative stress.

In the current study, two types of MGCs were observed within the testicular tissue. Multinucleated giant macrophages were mainly detected close to the lumen of seminiferous tubules. Their appearance may indicate an active inflammatory response to persistent tissue injury. Similar findings were reported previously, where such giant cells arise from the fusion of activated macrophages during chronic inflammation (Helming & Gordon, 2009). On the other hand, multinucleated germ cells were identified within the seminiferous tubules between germ cells, likely resulting from abnormal germ cell division. This interpretation agrees with previous research, suggesting that the formation of multinucleated spermatocytes and spermatids is due to defective mitosis or incomplete cytokinesis (Holstein & Eckmann, 1986). Taken together, these observations suggest that phthalate exposure triggers inflammatory and cytotoxic mechanisms. This leads to macrophage fusion and germ cell division disruption, thereby aggravating testicular injury.

Furthermore, the immunohistochemical findings offer molecular evidence supporting these structural alterations. In the present study, the observed reduction in inhibin-α and calretinin immunoexpression provides direct evidence of impaired Sertoli and Leydig cell functions. Inhibin-α is a well-established marker of Sertoli cell activity and reflects their ability to regulate spermatogenesis and maintain the intratesticular hormonal microenvironment (Naamneh Elzenaty et al., 2024). Therefore, its decline indicates Sertoli cell dysfunction. Unexpectedly, high-dose exposure induced intense yet aberrant inhibin-α immunoreactivity, reflecting a dysregulated, nonfunctional response of immature Sertoli cells under severe androgen deprivation. Under physiological conditions, adequate intratesticular testosterone supports Sertoli cell secretory trafficking (Mancuso et al., 2018) and, consequently, facilitates the release of inhibin-α into the circulation. These findings suggest that Sertoli cell dysfunction may underlie this decline and that intracytoplasmic accumulation of inhibin-α under high-dose exposure may be linked to testosterone deficiency, impairing androgen-dependent secretory trafficking. These findings are consistent with those reported by Demyashkin (2019) in cases of severe testicular disruption. Likewise, calretinin expression in the testis is closely associated with Leydig cell differentiation and steroidogenic activity, as it participates in calcium-dependent signaling pathways that are essential for androgen synthesis. Modulation of calretinin levels alters intracellular Ca^{2+} dynamics and the expression of steroidogenesis-related proteins, such as StAR, in Leydig cells (Xu et al., 2018). Decreased calretinin expression aligns with our earlier observation of lipid accumulation, reinforcing that Leydig cells are functionally compromised and unable to efficiently convert cholesterol into pregnenolone.

The present study found that phthalate exposure, especially DEHP, markedly increased PPAR-γ immunoreactivity in both Leydig and Sertoli cells, accompanied by ultrastructural evidence of lipid accumulation and peroxisome proliferation. These findings suggest altered lipid metabolism and cellular homeostasis in response to phthalate exposure. These findings are consistent with recent studies demonstrating that leptin increases lipid droplet content in Sertoli cells by upregulating PPAR-γ signaling (Dasso et al., 2026). Similarly, the increased PPAR-γ immunoreactivity observed in the present study was accompanied by lipid droplet accumulation, peroxisome proliferation, and mitochondrial and ER alterations. These alterations are consistent with previous reports describing their association with cellular stress and apoptosis-related signaling pathways (Zhou et al., 2025). However, pharmacological modulation of PPAR-γ can influence lipid metabolism and cellular stress responses in testicular cells (Zhang et al., 2023; Dasso et al., 2026), supporting its potential involvement.

Downloaded from academic.oup.com/mam/article/32/6/ozag107/8979578 by Ragesh Nair Nair on 17 November 2026

Likewise, activation of the PPARα/γ pathways has been reported in Sertoli cells, where it reprograms transcriptional activity and enhances ECM deposition (Froment et al., 2006). Excessive stimulation of the PPAR-γ axis under combined DEHP and microplastic exposure has also been associated with impaired lipophagy, lipid droplet accumulation, and increased oxidative stress, leading to aggravated testicular injury (Zhou et al., 2025). In addition, hepatic studies have shown that DEHP disrupts lipid metabolism through the LXR/SREBP-1c/PPARα/γ axis in cooperation with NF-κB signaling, promoting lipid accumulation and inflammatory responses (Huang et al., 2022). Overall, the present findings are consistent with the involvement of PPAR-γ in phthalate-induced testicular metabolic alterations, as evidenced by increased PPAR-γ immunoreactivity together with lipid accumulation and peroxisome proliferation. However, the molecular mechanisms underlying these alterations were not directly investigated and require further molecular studies.

Conclusion

DBP and DEHP exposure induced marked reproductive toxicity in male mice, leading to impaired spermatogenesis and persistent testicular alterations. Ultrastructural examination revealed mitochondrial damage, lipid accumulation, vacuolization, and fibrotic remodeling, while immunohistochemical analysis demonstrated altered inhibin-α, calretinin, and PPAR-γ expression, indicating disrupted Sertoli and Leydig cell function. Recovery following exposure cessation was dose-dependent and incomplete. Low-dose groups showed substantial functional recovery by 70 days of age, particularly in sperm concentration, whereas mid-dose groups exhibited delayed partial recovery. In contrast, high-dose groups showed persistent structural and functional impairment despite limited improvement at later ages. Overall, early-life exposure to DBP and DEHP resulted in long-lasting adverse effects on the male reproductive system.

Acknowledgments

The authors have no acknowledgments to declare.

Availability of Data and Materials

Correspondence and requests for materials should be addressed to Heba E. Aboulqasem.

Author Contributions Statement

R.A.A. did the conceptualization, data interpretation, writing—review & editing. D.F.M. involved in the review & editing. E.T.W. involved in the investigation (electron microscopy analysis). H.E.A. contributed to the investigation, methodology, data curation and interpretation, writing—original draft, and writing—review& editing. All authors read and approved the final version of the manuscript.

Financial Support

This research did not receive any specific grant from funding agencies in the public, commercial, or not-for-profit sectors.

Conflict of Interest

The authors declare that they have no known competing financial interests or personal relationships that could have appeared to influence the work reported in this paper.

Ethical Standards

The current study was achieved in accordance with the Egyptian laws and University guidelines for animal care. The National Ethical Committee of Assiut University, Faculty of Science Research Ethics Committee (FSREC), Egypt, has approved all the procedures in the present work with the approval number: 01-2025-0017.

References

Abd-Elmawla MA, Ghaiad HR, Abd Elbaqy YM, Zaki MB, Ismail RA, El-Shiekh RA & Gad ES (2026). Impact of endoplasmic reticulum (ER) stress on cellular functions and role of natural products as modulators. *Beni Suef Univ J Basic Appl Sci* **15**, 12. https://doi.org/10.1186/s43088-026-00736-z

Agency for Toxic Substances and Disease Registry (ATSDR). (2022). *Toxicological profile for di(2-ethylhexyl) phthalate (DEHP)*. U.S. Department of Health and Human Services. Available at https://www.ncbi.nlm.nih.gov/books/NBK590469. (retrieved September 2, 2026)

Aitken RJ (2024). The global decline in human fertility: The post-transition trap hypothesis. *Life* **14**, 369. https://doi.org/10.3390/life14030369

Al-Saleh I & Elkhatib R (2016). Screening of phthalate esters in 47 branded perfumes. *Environ Sci Pollut Res* **23**, 455–468. https://doi.org/10.1007/s11356-015-5267-z

Benjamin S, Masai E, Kamimura N, Takahashi K, Anderson RC & Faisal PA (2017). Phthalates impact human health: Epidemiological evidences and plausible mechanism of action. *J Hazard Mater* **340**, 360–383. https://doi.org/10.1016/j.jhazmat.2017.06.036

Beyer A, Schorgg P, Karavasiloglou N, Sarwar S, Rohrmann S, Bärnighausen T, Cassidy A, Connolly L & Kühn T (2022). Urinary phthalate concentrations and mortality risk: A population-based study. *Environ Res* **214**, 113927. https://doi.org/10.1016/j.envres.2022.113927

Chai X, Wen L, Song Y, He X, Yue J, Wu J, Chen X, Cai Z & Qi Z (2023). DEHP exposure elevated cardiovascular risk in obese mice by disturbing the arachidonic acid metabolism of gut microbiota. *Sci Total Environ* **875**, 162615. https://doi.org/10.1016/j.scitotenv.2023.162615

Chen X, Feng L, Xia Y, Li H, Liu F, Li Y, Xu H & Liu Y (2025). Exposure to tris(2,4-di-tert-butylphenyl) phosphate during adolescence induces testicular toxicity in mice: Autophagy-apoptosis interplay. *Ecotoxicol Environ Saf* **302**, 118598. https://doi.org/10.1016/j.ecoenv.2025.118598

Chiu K, Warner G, Nowak RA, Flaws JA & Mei W (2020). The impact of environmental chemicals on the gut microbiome. *Toxicol Sci* **176**, 253–284. https://doi.org/10.1093/toxsci/kfaa065

Dasso ME, Centola CL, Tabares FN, Galardo MN, Meroni SB & Riera MF (2026). Leptin increases lipid storage in Sertoli cells: Signaling pathways and cellular mechanisms involved. *Biochimie* **243**, 59–69. https://doi.org/10.1016/j.biochi.2026.01.009

Dees JH, Gazouli M & Papadopoulos V (2001). Effect of mono-ethylhexyl phthalate on MA-10 Leydig tumor cells. *Reprod Toxicol* **15**, 171–187. https://doi.org/10.1016/S0890-6238(01)00110-1

Demyashkin GA (2019). Inhibin B in seminiferous tubules of human testes in normal spermatogenesis and in idiopathic infertility. *Syst Biol Reprod Med* **65**, 20–28. https://doi.org/10.1080/19396368.2018.1478470

Downloaded from academic.oup.com/mam/article/32/6/ozag107/8979578 by Ragesh Nair Nair on 17 November 2026

Dong Y, Shu S, Yu X, Chen X, Li Q, Shen X & Yu Y (2025). Benzyl butyl phthalate promotes ferroptosis in Sertoli cells via disrupting ceruloplasmin-mediated iron balance. *Toxicology* **512**, 154078. https://doi.org/10.1016/j.tox.2025.154078

Emojevwe V, Naiho AO, Nwangwa EK, Oyovwi MO, Anachuna KK, Agbanifo-Chijiokwu E & Daubry TME (2022). Duration-dependent effects of high dose of phthalate exposure on semen quality in adult male rats. *JBRA Assist Reprod* **26**, 53–61. https://doi.org/10.5935/1518-0557.20210033

Eslami H, Nemati A, Jamshidi M, Ghaffarian-Bahraman A, Askari SG & Askari FR (2025). Exposure risks to phthalates by cosmetics and personal care products in pregnant women and early life: Urinary levels, mechanisms, biomarkers, and mitigation strategies: A review. *Chem Biol Interact*. **422**, 111786. https://doi.org/10.1016/j.cbi.2025.111786

European Chemicals Agency (ECHA) (2023). *Dibutyl phthalate (DBP): Registration dossier—toxicological information*. Helsinki, Finland. Available at https://chem.echa.europa.eu/100.001.416/dossier-view/b13234bf-2c9e-4393-8847-56d0e484afae

Froment P, Gizard F, Staels B, Dupont J & Monget P (2006). Peroxisome proliferator-activated receptors in reproductive tissues: From gametogenesis to parturition. *J Endocrinol* **189**, 199–209. https://doi.org/10.1677/joe.1.06667

Fu X, Han H, Li Y, Xu B, Dai W, Zhang Y, Zhou F, Ma H & Pei X (2021). Di-(2-ethylhexyl) phthalate exposure induces female reproductive toxicity and alters the intestinal microbiota community structure and fecal metabolite profile in mice. *Environ Toxicol* **36**, 1226–1242. https://doi.org/10.1002/tox.23121

Hassanin HM, Kamal AA & Ismail OI (2024). Resveratrol ameliorates atrazine induced caspase dependent apoptosis and fibrosis in the testis of adult albino rats. *Sci Rep* **14**, 17743. https://doi.org/10.1038/s41598-024-67636-z

Helming L & Gordon S (2009). Molecular mediators of macrophage fusion. *Trends Cell Biol* **19**, 514–522. https://doi.org/10.1016/j.tcb.2009.07.005

Holstein AF & Eckmann C (1986). Multinucleated spermatocytes and spermatids in human seminiferous tubules. *Andrologia* **18**, 5–16. https://doi.org/10.1111/j.1439-0272.1986.tb01729.x

Hsu SM, Raine L & Fanger H (1981). Use of avidin-biotin-peroxidase complex (ABC) in immunoperoxidase techniques: A comparison between ABC and unlabeled antibody (PAP) procedures. *J Histochem Cytochem* **29**, 577–580. https://doi.org/10.1177/29.4.6166661

Huang PC, Liao KW, Chang JW, Chan SH & Lee CC (2018). Characterization of phthalate exposure in cosmetics/perfume clerks. *Environ Pollut* **233**, 577–587. https://doi.org/10.1016/j.envpol.2017.10.079

Huang YQ, Tang YX, Qiu BH, Talukder M, Li XN & Li JL (2022). Di-2-ethylhexyl phthalate (DEHP) induced lipid metabolism disorder in liver via activating the LXR/SREBP 1c/PPARα/γ and NF κB signaling pathway. *Food Chem Toxicol* **165**, 113119. https://doi.org/10.1016/j.fct.2022.113119

Isobe T, Ohkawara S, Mori Y, Jinno H, Tanaka Kagawa T & Hanioka N (2023). Hydrolysis of dibutyl phthalate and di(2-ethylhexyl) phthalate in human liver, small intestine, kidney, and lung: An in vitro analysis using organ subcellular fractions and recombinant carboxylesterases. *Chem Biol Interact* **372**, 110353. https://doi.org/10.1016/j.cbi.2023.110353

Lei M, Menon R, Manteiga S, Alden N, Hunt C, Alaniz RC, Lee K & Jayaraman A (2019). Environmental chemical diethylhexyl phthalate alters intestinal microbiota community structure and metabolite profile in mice. *mSystems* **4**, e00724-19. https://doi.org/10.1128/msystems.00724-19

Li H & Spade DJ (2021). REPRODUCTIVE TOXICOLOGY: Environmental exposures, fetal testis development and function: Phthalates and beyond. *Reproduction* **162**, F147–F167. https://doi.org/10.1530/REP-20-0592

Li L, Huang L, Lei R, Zhang P, Yang Y, Liu H & Zhang Y (2024). DEHP and DBP, common phthalates, induce glucose metabolism disorders in rats via oxidative damage of PI3K/Akt/GLUT4 signaling. *Environ Pollut* **341**, 122948. https://doi.org/10.1016/j.envpol.2023.122948

Li X, Mo J, Zhu Q, Ni C, Wang Y, Li H, Lin ZK & Ge RS (2019). The structure-activity relationship (SAR) for phthalate-mediated developmental and reproductive toxicity in males. *Chemosphere* **223**, 504–513. https://doi.org/10.1016/j.chemosphere.2019.02.090

Mancuso F, Calvitti M, Milardi D, Grande G, Falabella G, Arato I, Giovagnoli S, Vincenzoni F, Mancini F, Nastruzzi C, Bodo M, Baroni T, Castagnola M, Marana R, Pontecorvi A, Calafiore R & Luca G (2018). Testosterone and FSH modulate Sertoli cell extracellular secretion: Proteomic analysis. *Mol Cell Endocrinol* **476**, 1–7. https://doi.org/10.1016/j.mce.2018.04.001

Mostafavi Abdolmaleky H & Zhou JR (2024). Gut microbiota dysbiosis, oxidative stress, inflammation, and epigenetic alterations in metabolic diseases. *Antioxidants* **13**, 985. https://doi.org/10.3390/antiox13080985

Naamneh Elzenaty R, Kouri C, Martinez de Lapiscina I, Sauter KS, Moreno F, Camats-Tarruella N & Flück CE (2024). NR5A1/SF-1 collaborates with inhibin α and the androgen receptor. *Int J Mol Sci* **25**, 10109. https://doi.org/10.3390/ijms251810109

National Toxicology Program (NTP). (2021). *NTP technical report on the toxicology and carcinogenesis studies of di-n-butyl phthalate (CASRN 84-74-2) administered in feed to Sprague Dawley (Hsd: Sprague Dawley® SD®) rats and B6C3F1/N mice*. NTP Technical Report No. 600. U.S. Department of Health and Human Services. https://doi.org/10.22427/NTP-TR-600

Nita TM, Wrobel SA, Vernez D, Koch HM, Wild P, Zufferey F, Rudaz S, Stenz L, Odermatt A & Hopf NB (2026). Hormonal changes in professional printers exposed to phthalates suggesting potential disturbances of the hypothalamic–pituitary–gonadal axis. *Environ Res* **291**, 123477. https://doi.org/10.1016/j.envres.2025.123477

Prasad B (2021). Phthalate pollution: Environmental fate and cumulative human exposure index using the multivariate analysis approach. *Environ Sci Process Impacts* **23**, 389–399. https://doi.org/10.1039/d0em00396d

Reddy BA, Venkataramanaiah P & Reddy MS (2025). Di-2-Ethylhexyl phthalate (DEHP) toxicity: Organ-specific impacts and human-relevant findings in animal models & humans—Review. *J Toxicol Risk Assess* **11**(1), 1–18. https://doi.org/10.23937/2572-4061.1510062

Rey RA (2021). The role of androgen signaling in male sexual development at puberty. *Endocrinology* **162**, bqaa215. https://doi.org/10.1210/endocr/bqaa215

Reynolds ES (1963). The use of lead citrate at high pH as an electron-opaque stain in electron microscopy. *J Cell Biol* **17**, 208–212. https://doi.org/10.1083/jcb.17.1.208

Seco Rovira V, Martínez Hernández J, Freire Brito L, Beltrán Frutos E, Madrid JF & Pastor LM (2025). Gradual thickening of the peritubular lamina propria in healthy boar seminiferous tubules due to cryptorchidism: Increased immunoexpression of diverse proteins in Sertoli and myoid cells. *Animals* **15**, 1696. https://doi.org/10.3390/ani15121696

Seed J, Chapin RE, Clegg ED, Dostal LA, Foote RH, Hurtt ME, Klinefelter GR, Makris SL, Perreault SL, Schrader S, Seyler D, Sprando R, Treinen KA, Veeramachaneni DN & Wise LD (1996). Methods for assessing sperm motility, morphology, and counts in the rat, rabbit, and dog: A consensus report. ILSI risk science institute expert working group on sperm evaluation. *Reprod Toxicol* **10**, 237–244. https://doi.org/10.1016/0890-6238(96)00028-7

Sharma A, Mollier J, Brocklesby RW, Caves C, Jayasena CN & Minhas S (2020). Endocrine-disrupting chemicals and male reproductive health. *Reprod Med Biol* **19**, 243–253. https://doi.org/10.1002/rmb2.12326

Strader LF, Linder RE & Perreault SD (1996). Comparison of rat epididymal sperm counts by IVOS HTM-IDENT and hemacytometer. *Reprod Toxicol* **10**, 529–533. https://doi.org/10.1016/S0890-6238(96)00140-2

Su H, Yuan P, Lei H, Zhang L, Deng D, Zhang L & Chen X (2022). Long-term chronic exposure to di-(2-ethylhexyl)-phthalate induces

Downloaded from academic.oup.com/mam/article/32/6/ozag107/8979578 by Ragesh Nair Nair on 17 November 2026

obesity via disruption of host lipid metabolism and gut microbiota in mice. *Chemosphere* **287**, 132414. https://doi.org/10.1016/j.chemosphere.2021.132414

Tian X, Yu Z, Feng P, Ye Z, Li R, Liu J, Hu J, Kakade A, Liu P & Li X (2019). Lactobacillus plantarum TW1-1 alleviates diethylhexyl phthalate-induced testicular damage in mice by modulating gut microbiota and decreasing inflammation. *Front Cell Infect Microbiol* **9**, 221. https://doi.org/10.3389/fcimb.2019.00221

Verma HP & Singh SK (2014). Effect of aqueous leaf extract of Dalbergia sissoo Roxb. On spermatogenesis and fertility in male mice. *Eur J Contracept Reprod Health Care* **19**, 475–486. https://doi.org/10.3109/13625187.2014.945165

Virant-Klun I, Imamovic Kumalic S & Pinter B (2022). From oxidative stress to male infertility: Review of the associations of endocrine disrupting chemicals (bisphenols, phthalates, and parabens) with human semen quality. *Antioxidants* **11**, 1617. https://doi.org/10.3390/antiox11081617

Wang J, Zhang X, Li Y, Liu Y & Tao L (2021). Exposure to Dibutyl phthalate and reproductive-related outcomes in animal models: Evidence from rodents study. *Front Physiol* **12**, 684532. https://doi.org/10.3389/fphys.2021.684532

Wang J-M, Li Z-F, Yang W-X & Tan F-Q (2022). Follicle-stimulating hormone signaling in Sertoli cells: A licence to the early stages of spermatogenesis. *Reprod Biol Endocrinol* **20**, 97. https://doi.org/10.1186/s12958-022-00971-w

Wang X, Yan X, Yang Y, Yang W, Zhang Y, Wang J, Ye D, Wu Y, Ma P & Yan B (2020). Dibutyl phthalate-mediated oxidative stress induces splenic injury in mice and the attenuating effects of vitamin E and curcumin. *Food Chem Toxicol* **136**, 110955. https://doi.org/10.1016/j.fct.2019.110955

Wowkonowicz P (2023). Phthalates in the environment: Their toxicology and associated risk to humans. *Environ Prot Nat Resour* **34**, 1–12. https://doi.org/10.2478/oszn-2023-0001

Xu W, Zhu Q, Liu S, Dai X, Zhang B, Gao C, Gao L, Liu J & Cui Y (2018). Calretinin participates in regulating steroidogenesis by PLC-Ca^{2+}-PKC pathway in Leydig cells. *Sci Rep* **8**, 7403. https://doi.org/10.1038/s41598-018-25427-3

Yang L, Liu S, Song P, Liu Z, Peng Z, Kong D, Zhou J, Yan X, Ma K, Yu Y, Liu X & Dong Q (2025). DEHP-mediated oxidative stress leads to impaired testosterone synthesis in Leydig cells through the cAMP/PKA/SF-1/StAR pathway. *Environ Pollut* **366**, 125503. https://doi.org/10.1016/j.envpol.2024.125503

Zakariah M, Molele RA, Mahdy MAA, Harande IS, Musa EZ, Dasa JJ & McGaw LJ (2025). Reproductive effects of dibutyl phthalate (DBP) toxicity in the testes of mammalian and avian species. *Toxicol Lett* **414**, 111779. https://doi.org/10.1016/j.toxlet.2025.111779

Zhang H, Ran M, Jiang L, Sun X, Qiu T, Li J, Wang N, Yao X, Zhang C, Deng H, Wang S & Yang G (2023). Mitochondrial dysfunction and endoplasmic reticulum stress induced by activation of PPARα led to testicular apoptosis in SD rats exposed to di-(2-ethylhexyl) phthalate (DEHP). *Ecotoxicol Environ Saf* **268**, 115711. https://doi.org/10.1016/j.ecoenv.2023.115711

Zhou X, Yan H, Hong Y, Ding Y, Chen J, Tang H, Wei Y, Long C, Shen L, Wei G & Wu S (2025). PPARγ mediated lysosomal membrane permeabilization and lipophagy blockage were involved in microplastics and di(2-ethylhexyl) phthalate co-exposure induced immature testis injury. *Free Radic Biol Med* **237**, 615–630. https://doi.org/10.1016/j.freeradbiomed.2025.06.023

Downloaded from academic.oup.com/mam/article/32/6/ozag107/8979578 by Ragesh Nair Nair on 17 November 2026